

3841

# SANDIA REPORT

SAND87-1433 • UC-70

Unlimited Release

Printed December 1988

ZIMMERMAN  
ET AL

Yucca Mountain Project

## G-Tunnel Welded Tuff Mining Experiment Evaluations

Roger M. Zimmerman, Robert A. Bellman, Jr., Kevin L. Mann,  
Daniel P. Zerga, Matthew Fowler, Roy L. Johnson

Prepared by  
Sandia National Laboratories  
Albuquerque, New Mexico 87185 and Livermore, California 94550  
for the United States Department of Energy  
under Contract DE-AC04-76DP00789

"Prepared by Yucca Mountain Project (YMP) participants as part of the Civilian Radioactive Waste Management Program (CRWM). The YMP is managed by the Yucca Mountain Project Office of the U. S. Department of Energy, Nevada Operations Office (DOE/NV). YMP work is sponsored by the Office of Geologic Repositories (OGR) of the DOE Office of Civilian Radioactive Waste Management (OCRWM)."

Issued by Sandia National Laboratories, operated for the United States Department of Energy by Sandia Corporation.

**NOTICE:** This report was prepared as an account of work sponsored by an agency of the United States Government. Neither the United States Government nor any agency thereof, nor any of their employees, nor any of their contractors, subcontractors, or their employees, makes any warranty, express or implied, or assumes any legal liability or responsibility for the accuracy, completeness, or usefulness of any information, apparatus, product, or process disclosed, or represents that its use would not infringe privately owned rights. Reference herein to any specific commercial product, process, or service by trade name, trademark, manufacturer, or otherwise, does not necessarily constitute or imply its endorsement, recommendation, or favoring by the United States Government, any agency thereof or any of their contractors or subcontractors. The views and opinions expressed herein do not necessarily state or reflect those of the United States Government, any agency thereof or any of their contractors or subcontractors.

Printed in the United States of America  
Available from  
National Technical Information Service  
U.S. Department of Commerce  
5285 Port Royal Road  
Springfield, VA 22161

NTIS price codes  
Printed copy: A10  
Microfiche copy: A01

DRAFT  
SAND87-1433

G-TUNNEL WELDED TUFF MINING EXPERIMENT EVALUATIONS

by

Roger M. Zimmerman  
Sandia National Laboratories  
Albuquerque, NM

Robert A. Bellman, Jr., and  
Kevin L. Mann  
Science Applications International Corporation  
Las Vegas, NV

Daniel P. Zerga and  
Matthew Fowler  
Parsons Brinckerhoff Quade and Douglas  
San Francisco, CA

Roy L. Johnson  
University of New Mexico  
Albuquerque, NM

ABSTRACT

Designers and analysts of radioactive waste repositories must be able to predict the mechanical behavior of the host rock. Sandia National Laboratories elected to conduct a mine-by in welded tuff so that predictive-type information could be obtained regarding the response of the rock to a drill and blast excavation process, where smooth blasting techniques were used. This report describes the results of the mining processes and presents and discusses the rock mass responses to the mining and ground support activities.

Data was gathered and  
analyses performed at  
Quality Assurance Level III

## CONTENTS

	<u>Page</u>
1.0 INTRODUCTION .....	1-1
1.1 Purpose of Document .....	1-1
1.2 Background .....	1-1
2.0 MINING AND GROUND SUPPORT EVALUATIONS .....	2-1
2.1 Smooth Blasting Evaluations .....	2-1
2.2 Ground Support Design .....	2-4
2.2.1 Drift Design .....	2-4
2.2.2 Drift Design Approach .....	2-6
2.2.3 Design Applications .....	2-9
2.2.3.1 Shape Considerations .....	2-9
2.2.3.2 Ground Support .....	2-10
2.2.4 Ground Support Discussions .....	2-14
3.0 DRIFT CONVERGENCE BEHAVIOR .....	3-1
3.1 Drift Convergence Magnitudes .....	3-1
3.1.1 Tape Extensometer Measurements .....	3-1
3.1.2 Multiple-Point Borehole Extensometer Measurements .....	3-2
3.1.3 Convergence Magnitude Discussions .....	3-4
3.1.3.1 Comparisons of Tape Extensometer and Multiple-Point Borehole Extensometer Measurements .....	3-4
3.1.3.2 Comparisons of Measured Convergence and Model Predictions .....	3-8
3.1.3.3 Comparisons of Measurements With Case History Criteria .....	3-11
3.2 Drift Convergence Rates .....	3-12
3.2.1 Tape Extensometer Measurements .....	3-12
3.2.2 Multiple-Point Borehole Extensometer Measurements .....	3-12
3.2.3 Convergence Rate Discussions .....	3-13
3.3 Support Displacement Capacities .....	3-14
3.4 Drift Convergence Summary .....	3-16

CONTENTS  
(Continued)

	<u>Page</u>
4.0 RELAXED ZONE AND RELATED ROCK MASS EVALUATIONS .....	4-1
4.1 Relaxed Zone Description .....	4-1
4.1.1 Stress Redistributions .....	4-2
4.1.2 Blast Damage .....	4-3
4.1.3 Other Relaxed Zone Determinations .....	4-4
4.2 Relaxed Zone Evaluations Using Hydraulic Quotient Measurements .....	4-5
4.2.1 Borehole Injection Testing Background .....	4-5
4.2.2 Hydraulic Quotient Measurements .....	4-7
4.3 Relaxed Zone Evaluations Using Multiple-Point Borehole Extensometer Measurements .....	4-10
4.3.1 Multiple-Point Borehole Extensometer Measurement Background .....	4-10
4.3.2 Multiple-Point Borehole Extensometer Measurements .....	4-12
4.4 Summary of Relaxed Zone Evaluations .....	4-17
4.5 Rock Mass Measurement/Model Comparisons .....	4-19
4.6 Rock Mass Hydraulic Properties .....	4-24
4.6.1 Aperture Changes .....	4-24
4.6.2 Conversion of Hydraulic Quotient Measurements to Permeability Values .....	4-27
5.0 SUMMARY, CONCLUSIONS, AND RECOMMENDATIONS .....	5-1
5.1 Summary for Evaluation of the Rock Performance During Excavation .....	5-1
5.1.1 Evaluation of Drift Convergence Phenomena .....	5-1
5.1.2 Design of Predictive Capabilities .....	5-2
5.1.3 Application of Control Blasting Technique .....	5-3
5.1.4 Conclusions on Performance of Rock During Excavation .....	5-4
5.1.5 Recommendations for Future Rock Excavation Studies .....	5-5

CONTENTS  
(Concluded)

	<u>Page</u>
6.0 REFERENCES .....	6-1
APPENDIX A TWO-DIMENSIONAL LINEAR ELASTIC MODEL PREDICTIONS .....	A-1
A.1 Drift Convergence Modeling .....	A-2
A.1.1 Two-Dimensional Model .....	A-2
A.1.2 Model Limitations .....	A-5
A.1.3 Model Results .....	A-6
APPENDIX B RIB/SEPDB DATA.....	B-1

## FIGURES

<u>Figure</u>	<u>Page</u>
1-1 Plan View of Demonstration Drift Details Associated with Welded Tuff Mining Experiment .....	1-3
1-2 Elevation View Showing Location of Instrumentation and Measurement Holes Relative to Major Drifts with Typical Geologic Features .....	1-3
2-1 Plan View of Blast Rounds.....	2-2
2-2 Comparisons of Rock Mass Classifications and Typical Ground Support Classifications .....	2-8
2-3 Typical Ground Supports for Horizontal Configuration .....	2-11
2-4 Final Ground Support for Demonstration Drift .....	2-13
3-1 Summary of Vertical Tape Extensometer Data.....	3-3
3-2 Summary of Horizontal Tape Extensometer Data .....	3-3
3-3 Vertical Multiple-Point Borehole Extensometer Displacement Histories at Station C and E .....	3-5
3-4 Horizontal Multiple-Point Borehole Extensometer Displacement Histories at Stations C and E .....	3-6
4-1 Plots of Pre- and Postmining Hydraulic Quotient Quantities for Welded Tuff Above Demonstration Drift .....	4-8
4-2 Comparisons of Roof Multiple-Point Borehole Extensometer Data and Model Results for J-Day 145 (1986) .....	4-13
4-3 Comparisons of Floor Multiple-Point Borehole Extensometer Data and Computer Output for J-Day 145 (1986) .....	4-14
4-4 Comparisons of Horizontal Multiple-Point Borehole Extensometer Data and Computer Output for J-145 (1986) .....	4-15
A-1 Mesh for Welded Tuff Mining Evaluations--Linear Elastic Model .....	A-3
A-2 Vertical Displacement Profile Along Centerline of Demonstration Drift .....	A-7
A-3 Bottom Anchor Relative Predicted Multiple-Point Borehole Extensometer Displacement Profiles in Vertical Direction .....	A-8
A-4 Horizontal Displacement Profile at Mid-Height of Demonstration Drift .....	A-10
A-5 Bottom Anchor Relative Predicted Multiple-Point Borehole Extensometer Displacement Profiles in Horizontal Direction .....	A-11
A-6 Predicted Stress Distributions Around Demonstration Drift .....	A-12

TABLES

<u>Table</u>		<u>Page</u>
2-1	Summary of Problems Found in Demonstration Drift Mining .....	2-5
2-2	Applications of Rock Mass Classification Systems to G-Tunnel Tuffs .....	2-7
3-1	Summary of Measured Drift Convergence Magnitudes .....	3-2
3-2	Summary of Predicted Drift Convergence Magnitudes .....	3-10
3-3	Summary of Measured Drift Convergence Rates .....	3-13
4-1	Summary of Premining Hydraulic Quotient Measurements in Welded Tuff .....	4-26
A-1	Material Properties for Numerical Model .....	A-4

## ACKNOWLEDGEMENTS

The authors are indebted to many for their contributions to these welded tuff mining evaluations. In particular, we wish to acknowledge contributions from the following persons:

### From Sandia National Laboratories

Robert L. Schuch	For an excellent job of coordinating activities of personnel from SNL, SAIC, PBQ&D, and REECo
Joe Bradshaw	For exceptional dedication in the preparation of equipment and collection of the permeability data as well as overall support for the needs of the program
Carl Denney	For technical expertise leading to the setup of the data acquisition system and the conversion of Irad gages from manual to monitored measurements
John Talbutt	For very helpful assistance in G-Tunnel operations and logistics
Les Shephard	For extremely helpful comments and criticisms in the peer review
Larry Costin	For extremely helpful comments and criticisms in the peer review

### From Science Applications International Corporation

Mike Allen	For exceptional dedication in the tape extensometer data collection and the installation of field instruments
Brian Keohi	For diligence in support of laboratory and field data collection

### From Persons Brinckerhoff Quade and Douglas

Will Streeter	For generous applications of talents in mining activities
---------------	---

### From EG&G

Don Mason	For skill in developing the software for the data acquisition system and help in keeping it operating
-----------	---

### From Fenix and Scisson

Mike O'Brien	For continued support in geologic interpretations
--------------	---

From REECo

Don Hembre	For assistance as REECO project manager in the planning and conduct of the drilling and mining activities
Lavel Atkinson	For assistance as REECO tunnel superintendent in the planning and conduct of the drilling and mining activities
Sam Williams	For very helpful assistance in the planning and conduct of the field activities
Miners and Drillers	For their cooperation and patience in doing a nontraditional job to support underground research

## 1.0 INTRODUCTION

### 1.1 Purpose of Document

This report is the third in a series of four covering the G-Tunnel Welded Tuff Mining (WTM) Experiment. The first report (Zimmerman et al., in prep. a), covering experiment preparations, contains background rationale and provides the purpose of the experiment. The first report also provides details of the measurement systems and includes topics on measurement principles, measurement equipment, and installation details and procedures. The second report (Zimmerman et al., in prep. b) provides the data summary in engineering units. Included in the report are calibration data and error analyses for new developmental efforts.

The purpose of this third report is to provide evaluations of the WTM experiment with emphasis on the rock mass behavior. Major subjects discussed are (1) mining and ground support design, (2) drift convergence phenomena, and (3) relaxed zone behavior. Many of the details in the first two reports are not repeated here. Appropriate figures and data are repeated and pertinent details are liberally referenced to the preparation and data summary reports, which are identified as Report A and Report B. A fourth report discusses evaluations of the measurement systems (Zimmerman et al., in prep. c) and is identified as Report C.

### 1.2 Background

The WTM experiment was conducted in the G-Tunnel Underground Facility (GTUF) using two drifts (Report A). Figure 1-1 shows a plan view of the two drifts. The first drift constructed was the 12-Drift extension. The 12-Drift served as the observation drift, where boreholes were drilled into the rock mass into which the Demonstration Drift would be mined. These boreholes were used for measurements before, during, and after the excavation of the Demonstration Drift.

Figure 1-1 shows the measurement stations that were used for both the Demonstration Drift and 12-Drift. Pertinent dimensions are shown in the figure. Measurements were normally identified with stations, which were identified with mining rounds. Two stations, C and E, were located at predetermined distances in the Demonstration Drift because of the presence of station-dependent instrumentation originating from the 12-Drift.

Also shown in Figure 1-1 are the major geologic features, including a fault and fractures. These were visually mapped from the inside of the drift by the authors. The unnamed normal fault (Strike N 50° W, dip 85°, displacement ~2.5 m) was also observed in the 12-Drift, where it has a 3.6-m displacement as determined by a G-Tunnel geologist. Major fractures are also shown in Figure 1-1. The fractures dip sub-vertically.

Figure 1-2 shows a representative elevation view of the two drifts with pertinent dimensions and major instrumentation positions (Report A). Multiple-point borehole extensometers (MPBXs), with origins in the Demonstration Drift, were located in Positions 1 through 6, and MPBXs were located with origins in the 12-Drift and identified with Position 7. MPBXs were located only at Stations C and E. MPBXs are identified by station and position number, thus a vertical MPBX oriented up at Station C would be identified as MPBX C3.

The four long boreholes originating from the 12-Drift, identified by 1 through 4 in Figure 1-2, were located at Stations B, D, and F. These boreholes were used for special types of pre- and postmining measurements. Measurements in the steepest borehole at Station B would be identified as Borehole B1.

The Demonstration Drift was located in multilayered tuff as shown in Figure 1-2 (Report A). Because of the fault, the floor of the drift was located in the bottom of the densely welded tuff, the rubble zone, and the vitric welded tuff.

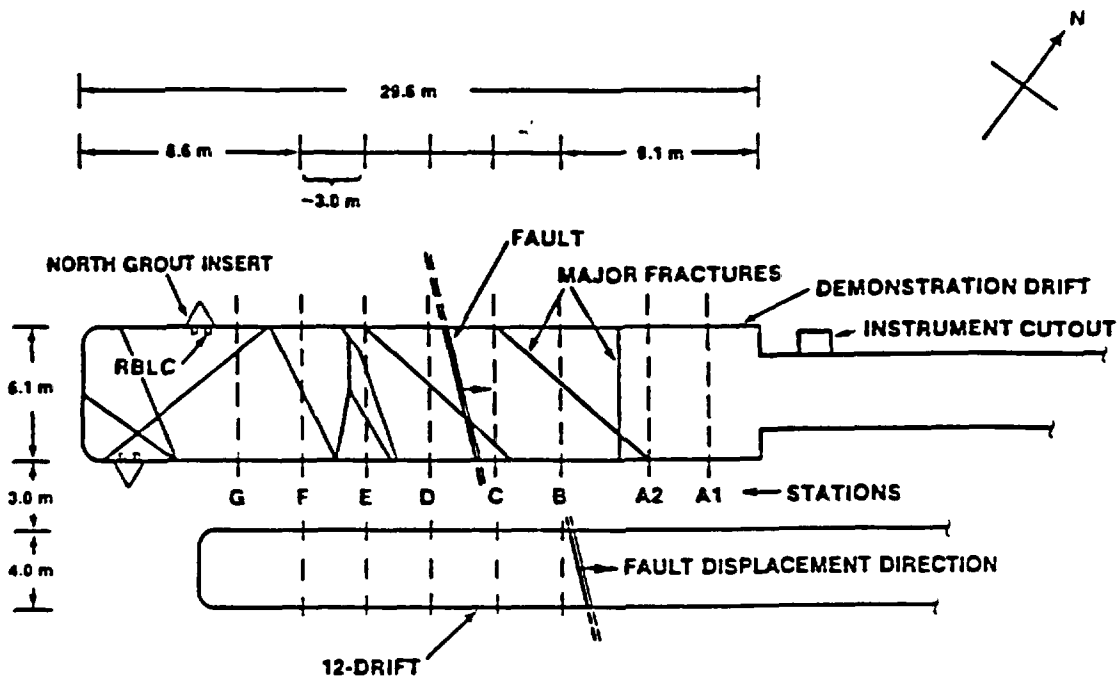


Figure 1-1. Plan View of Demonstration Drift Details Associated with Welded Tuff Mining Experiment

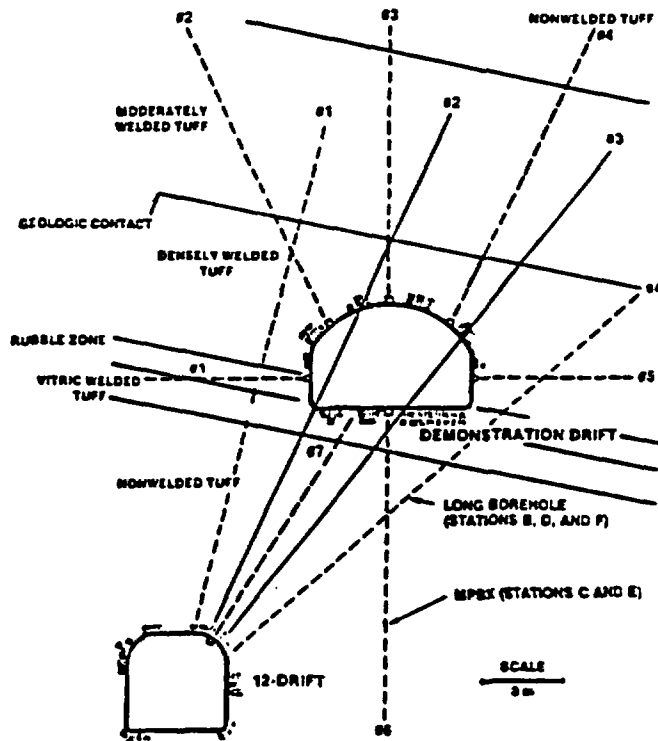


Figure 1-2. Elevation View Showing Location of Instrumentation and Measurement Holes Relative to Major Drifts with Typical Geologic Features

## 2.0 MINING AND GROUND SUPPORT EVALUATIONS

The construction of the Demonstration Drift represents the first documented effort of mining in welded tuff to gain experience for possible repository applications. The drift was sized with dimensions similar to some drifts planned for repository drifts to provide Yucca Mountain Project (YMP) engineers full-scale field experiences for use in later Exploratory Shaft (ES) and ongoing repository designs. A recognized limit to the mining in the GTUF was that the Demonstration Drift would have to be short, 29.6 m long. This meant that there would be limited opportunities to optimize blast and ground support designs.

### 2.1 Smooth Blasting Evaluations

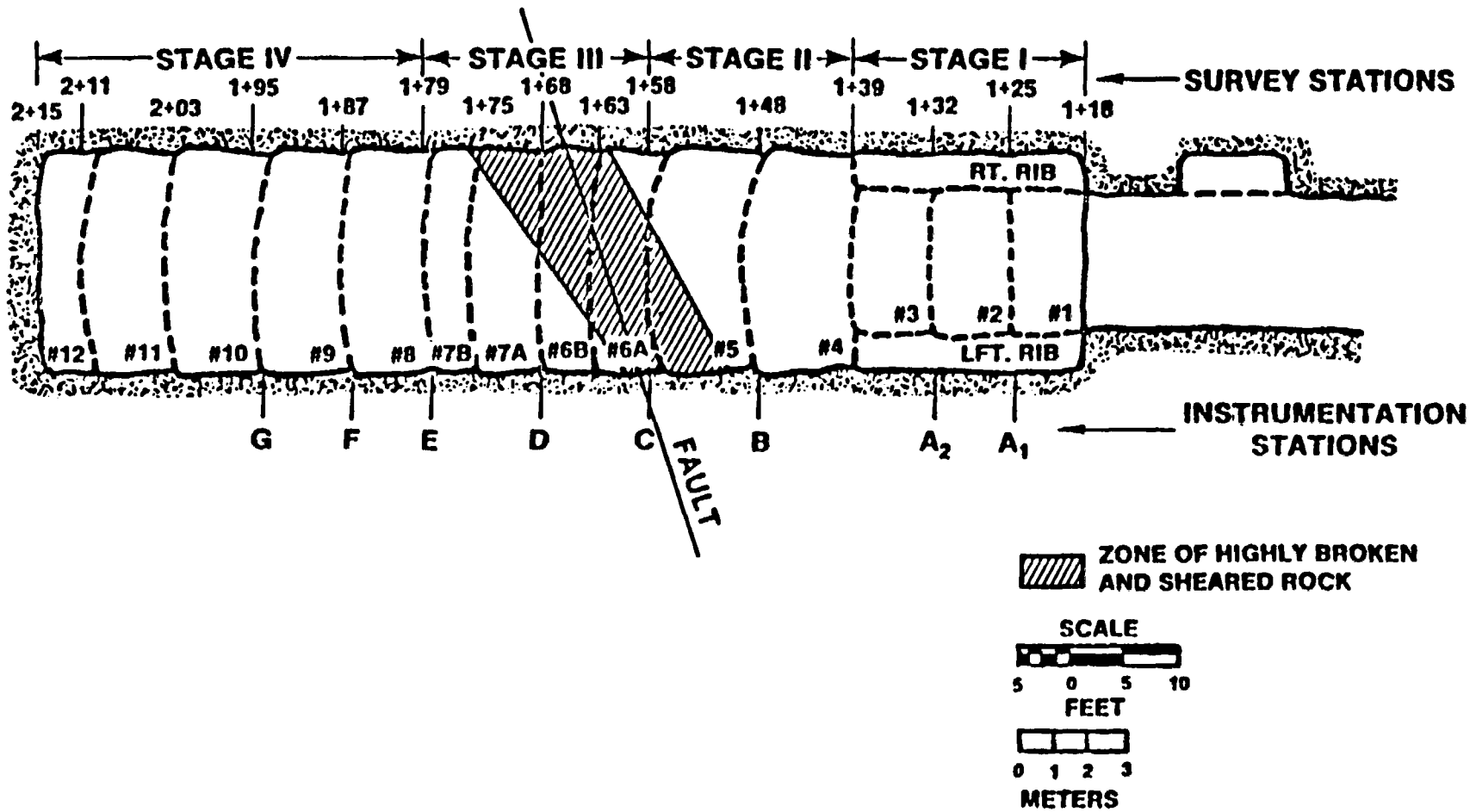
Hoek and Brown (1980) discuss blasting in underground applications and indicate that smooth blasting and presplitting are two techniques commonly used to minimize crack propagation around the designed perimeter of an excavation. Presplitting is slower than smooth blasting because of the need for an extra step in the mining cycle. Personnel from Parsons Brinckerhoff Quade and Douglas (PBQ&D) were involved in the planning, fielding, and evaluations of this experiment and recommended applications of smooth blasting techniques for this first effort. They recommended three major objectives (Report A\*), which were

- (1) obtain a low level of overbreak and damage to the surrounding rock,
- (2) attain a 3-m full-face advance, and
- (3) evaluate fragmentation.

Figure 2-1 summarizes the actual blast rounds. Rounds are identified by number. The mining was conducted in four stages (see Report A for details). Stage I consisted of three smaller size rounds followed by

---

\*Zimmerman et al., in prep. a.



2-2

Figure 2-1. Plan View of Blast Rounds

additional removal of the right and left ribs. The smaller size rounds were used to gain familiarization with the welded tuff. Stage II was the start of full-face mining. Stage II terminated at Station C, where MPBXs were to be installed. Stage III consisted of shorter rounds to serve two purposes. First, it was decided that rounds between C and E would be short rounds so that the drift convergence studies would be enhanced. Second, it was observed that the rock quality was deteriorating somewhat because of the presence of the fault beyond C. Special burn and V cuts were used in Stage III to address this second problem. Stage IV consisted of five rounds to complete the Demonstration Drift. Because of equipment problems, the last five rounds were nominally 2.4-m rounds rather than the 3.0-m rounds used in Stage II.

Evaluations of the first mining objective on perimeter control are somewhat subjective. Data pertaining to the blasting activities and photographs of the drift surfaces are contained in Report B and are not repeated here. The photographs show that the shape was as desired and that there was some evidence of desired perimeter control, as evidenced by the presence of portions of the perimeter drill holes on the drift surface. The overall perimeter control was determined from the initial distances for the tape convergence measurements anchors. The average vertical measurement was  $3.94 \pm 0.20$  m, based on measurements at eleven stations, and the average horizontal measurement was  $6.12 \pm 0.14$  m, based on measurements at 8 stations. There were variations in the drift surface between convergence measurement anchors, with the largest occurring in the vicinity of the fault. An overbreak of approximately 0.6 m was observed in the roof in this region.

The second objective was to evaluate the practicality of full-face mining. Full-face mining is facilitated with the use of a twin boom jumbo, and a used jumbo was rented for this mining. Using the jumbo, the estimated time for mining a 3.0-m round without difficulties was 800 min (Report B\*\*). There was some down time in the mining that is discussed here but this would be expected to be reduced in mining longer drifts.

---

\*\*Zimmerman et al., in prep. b.

The down time was partly due to the condition of the used equipment available for the mining and partly due to problems occurring during drilling and blasting activities. Table 2-1 summarizes the major problems that were observed during the mining. Probable causes for the problems are noted in the table. Most of the problems contributed to an underbreak, which was easily cleaned up with secondary blasting. Secondary blasting activities were considered as part of the down time. Most of the rock quality probable causes in Table 2-1 occurred in the fault zone.

The final objective was to evaluate fragmentation patterns for designing muck removal and dust collection systems. Data are contained in Report B. In the report, the data showed that a large percentage (50% by weight) of the blasted rock passed the 5.1-cm opening. The results were most likely impacted by the presence of the rubble zone in the round that was selected (#10). The rubble zone is composed of angular rock fragments with a fine-grained matrix; the latter probably produced most of these fines. The relatively high amount of fines did not appear to cause dust control problems; however, significant postblast ventilation of the face was necessary. On the other end of the scale, there was a relatively small percentage (16%) of larger fragments that did not pass the 20.3-cm opening. The largest rock in this round measured 51 x 30 x 15 cm (20 x 12 x 6 in.). The muck fragment distributions were easily handled by 3.8-m<sup>3</sup> load-haul-dump equipment available in G-Tunnel. Belt feeders could be designed to handle muck fragments of this size.

## 2.2 Ground Support Design

### 2.2.1 Drift Design

The construction of the Demonstration Drift provided an opportunity to apply and review ground support techniques. The drift was too short to try a number of ground support concepts and evaluate the best one; therefore, one system was selected as the basic ground support system and then there were four limited-scale variations to demonstrate applicability to welded tuff.

TABLE 2-1

SUMMARY OF PROBLEMS FOUND IN DEMONSTRATION DRIFT MINING

<u>Round(s)</u>	<u>Observed Problem</u>	<u>Probable Causes</u>
<u>Before Blasting</u>		
5,6A	Holes not to specified depths	Miner error, collapsing hole
5,6A,7A,8	Holes caved in during drilling	Rock quality
5,6A,7A	Drilling water detoured to nearby holes or circulation was lost	Rock quality
2,4,7A	Drill holes not straight	Miner error
1,2,4,6A,7A,10	Holes not at specified locations	Miner error, rock quality, jumbo limitations
<u>After Blasting</u>		
2,3,4,7A,7B,8	Perimeter explosives did not pull full depth	Improper explosive placement, inaccurate hole alignment and depth, possible errors in delay cap blasting times
1,2,3,8	Perimeter holes did not form a smooth break surface	Poor hole alignment, inaccurate hole alignment and depth, powder factor, rock quality
3,4,5	Explosives were pulled from holes by other detonations	Improper stemming, rock quality
4	Explosives were improperly primed	Improper explosive placement
4	Incomplete detonation	Improper explosive placement
6B,7A	Overbreak	Rock quality, perimeter powder concentrations

### 2.2.2 Drift Design Approach

The design approach was to apply empirical methods to predict the behavior of the rock mass and ground support on the basis of rock mass classifications. It was recognized that the empirical methods are the most useful for predicting the initial ground support requirements and that in many cases the ground support may be changed based on in situ evaluations. In experiment planning, the excavation of the Demonstration Drift was to be monitored with drift convergence measurements to check the adequacy of the proposed ground support design.

Two prominent rock mass classification systems are the NGI(Q) System (Barton et al., 1974) and the CSIR System (Bieniawski, 1976). Each is based on the premise that a successful support system design is attributed to the effectiveness of geological investigations and on the ability to extrapolate past experiences of support performance to new rock mass environments. Rock mass classifications for the welded and nonwelded tuffs in G-Tunnel had been prepared by Langkopf and Gnirk (1986). The tuffs were classified by procedures applicable to both systems, as shown in Table 2-2. It was assumed that the classifications were applicable to the Demonstration Drift.

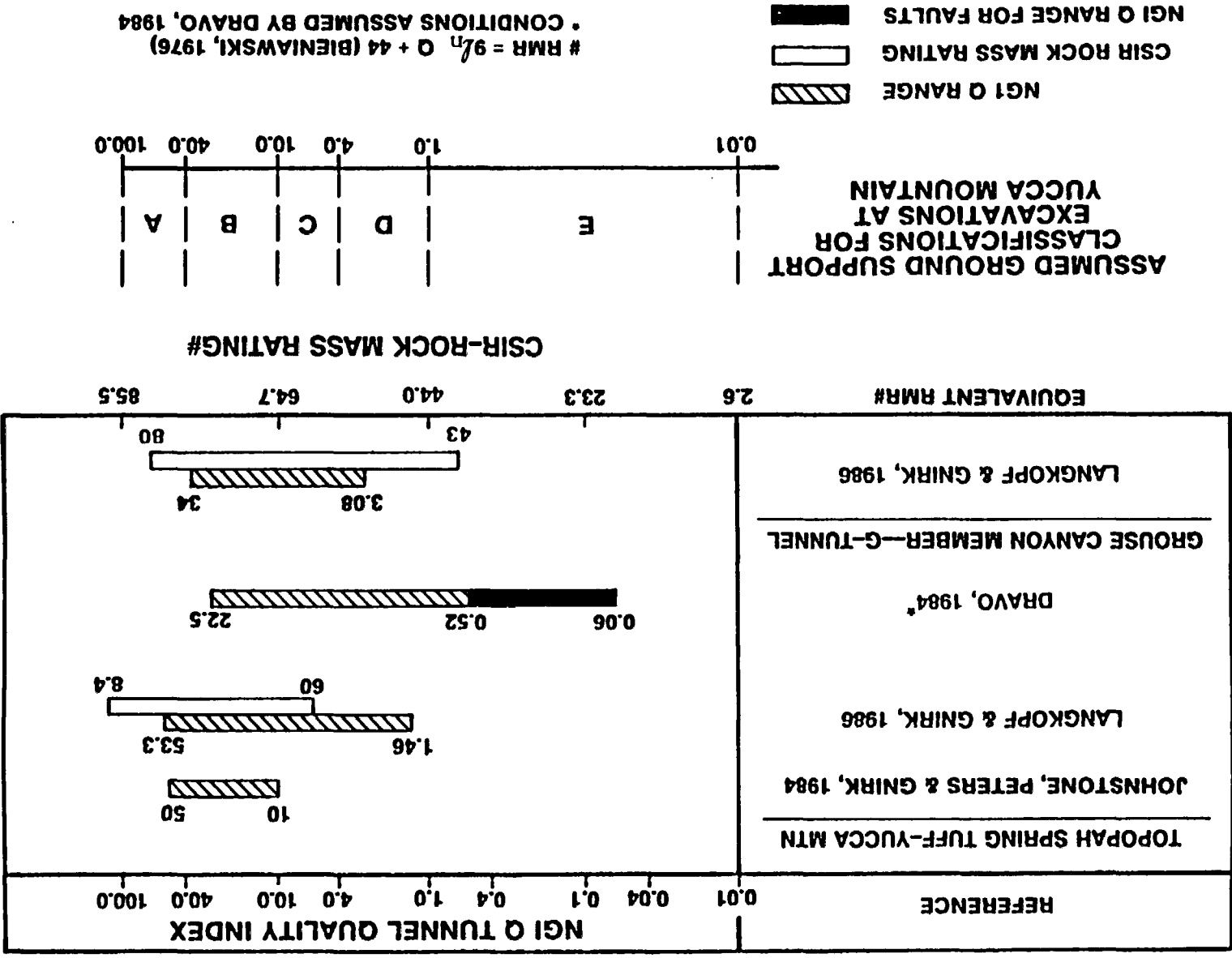
Figure 2-2 shows the range of reported values for the two systems for welded and nonwelded tuffs. Included in the figure are rock mass classification representations of welded tuffs at G-Tunnel and Yucca Mountain so that a comparison can easily be made. The CSIR rating is also placed on the figure, as per Bieniawski (1976). Figure 2-2 shows assumed rock categories that are used to classify different roof support designs for the conceptual repository. The different supports are discussed in the next section.

TABLE 2-2

## APPLICATIONS OF ROCK-MASS CLASSIFICATION SYSTEMS TO G-TUNNEL TUFFS (Langkopf and Gnirk, 1986)

System	Tuff	Parameter	Pertinent Input	Final Rating
CSIR	Welded	Strength of Intact Rock	Compressive Strength = 110 MPa	7-12
	Nonwelded		Compressive Strength = 15 MPa	1-2
	Welded	Drill Core Quality (RQD)	RQD = 37-51	8-13
	Nonwelded		RQD = 93	20
	Welded	Spacing of Joints	Joint Frequency = 3.0-4.5 f/m	10-20
	Nonwelded		Joint Frequency = 0.5-1.0 f/m	20-25
	Welded	Conditions of Joints	Very rough surfaces, not continuous, no separation, hard joint wall rock to slightly rough surfaces, separation < 1 mm	20-25
	Nonwelded		Slightly rough surfaces, separation < 4 mm, soft joint wall rock	12
	Welded	Groundwater	None	10
	Nonwelded		None	10
	Welded	Rock Mass Rating (RMR)	---	43-80
	Nonwelded		---	51-69
	NGI	Welded	Rock Quality Designation	RQD = 37-51
Nonwelded		RQD = 93		93
Welded		Joint Set Number	2 to 3 joint sets + random	6-12
Nonwelded			Massive, no or few joints	0.5-1.0
Welded		Joint Roughness Number	Discontinuous joints to smooth, undulating	4.0-2.0
Nonwelded			Smooth, undulating to smooth, planar	2.0-1.0
Welded		Joint Alteration Number	Unaltered joint walls, surface straining only to slightly altered joint walls	1.0-2.0
Nonwelded			Unaltered joint walls, surface straining only to slightly altered joint walls	1.0-2.0
Welded		Joint Water Reduct. Number	---	1.0
Nonwelded			---	1.0
Welded		Stress Reduction Factor	Overburden Stress = 6.0-8.2	1.0
Nonwelded			Overburden Stress = 6.0-8.2	1.0
Welded		Q-Rating	---	34.0-3.08
Nonwelded	---		46.5-0.24	

Figure 2-2. Comparisons of Rock Mass Classifications and Typical Ground Support Classifications



### 2.2.3 Design Applications

#### 2.2.3.1 Shape Considerations

The shape of the drift was selected by PBQ&D to approximate the general shape of large scale drifts planned for a repository. An arched shape was recommended because of the stress conditions and the recognition that the arch shape favors openings with predominately vertical stress loadings.

Stresses, geology, and clearance considerations led to the final shape of the Demonstration Drift. Zimmerman and Vollendorf (1982) reported the results of in situ stress measurements in G-Tunnel. When these stresses were transformed to conform to the bearing of the Demonstration Drift, the horizontal normal stress in a direction perpendicular to the drift was -1.7 MPa and the vertical stress was -7.1 MPa (tension is assumed positive). The ratio of the horizontal to vertical stress becomes  $1.7/7.1 = 0.24$ . For a repository conceptual design with a stress ratio of this magnitude, PBQ&D engineers recommended a ratio of radius of curvature/width ( $R_c$ ) of about 0.6 to achieve a reasonable stress distribution around the perimeter.

For a 6.1-m width, the radius would be 3.7 m using the 0.6 factor. The spring line for this radius would be 2.1 m above the floor. It was desirable to have the spring line at a height of 2.4 m to minimize disturbance in the rubble zone on the high side of the fault and to allow more clearance for the large drill jumbo. Consideration of these factors led to a design of a drift with a height of 4.0 m and spring lines at the 2.4-m height. This corresponds to an  $R_c$  ratio of 0.72. In general, repository thermal considerations would cause the horizontal stresses to be higher so that  $R_c$  would be larger than for the ambient temperature condition; thus, the adjustment was assumed to be in an acceptable direction.

### 2.2.3.2 Ground Support

The assumed ground support classifications in Figure 2-2 have been translated to different support designs by PBQ&D and preliminary designs for a representative repository opening 9.4 m wide are shown in Figure 2-3. At the time of the design for the Demonstration Drift (circa 1985), a repository drift that wide was being considered for an alcove for horizontal canister emplacement. The alcoves would be used as locations of horizontal emplacement holes and would be spaced at regular intervals. The alcoves would be separated with drifts nominally 6.1 m wide, the design dimensions for the Demonstration Drift. The different types of support would be the following:

<u>PBQ&amp;D Classification</u>	<u>Ground Support Description</u>
A	Friction-type rock bolts as needed for conditions
B	Welded wire mesh as needed in crown with grouted dowels in a pattern in crown and upper half of sidewall
C	Welded wire mesh in crown and sides, supported by grouted dowels placed in a pattern and 76 mm (3 in.) of shotcrete
D	Initial support-friction-type bolts with 76 mm (3 in.) of steel fiber-reinforced shotcrete. Final support/grouted dowels (placed in a pattern), welded wire mesh, and 76 mm (3 in.) of additional shotcrete

Three considerations led to the selection of ground support classification B for the Demonstration Drift. The first was the rock mass classification where a class B support would be at the upper end of the ranges in both systems. The second was the evidence in G-Tunnel that rock bolts and wire mesh had proved to be satisfactory for drifts up to 4.9 m wide in moderately welded tuff. The third was the nominal rule of thumb used in

# HORIZONTAL CONFIGURATION

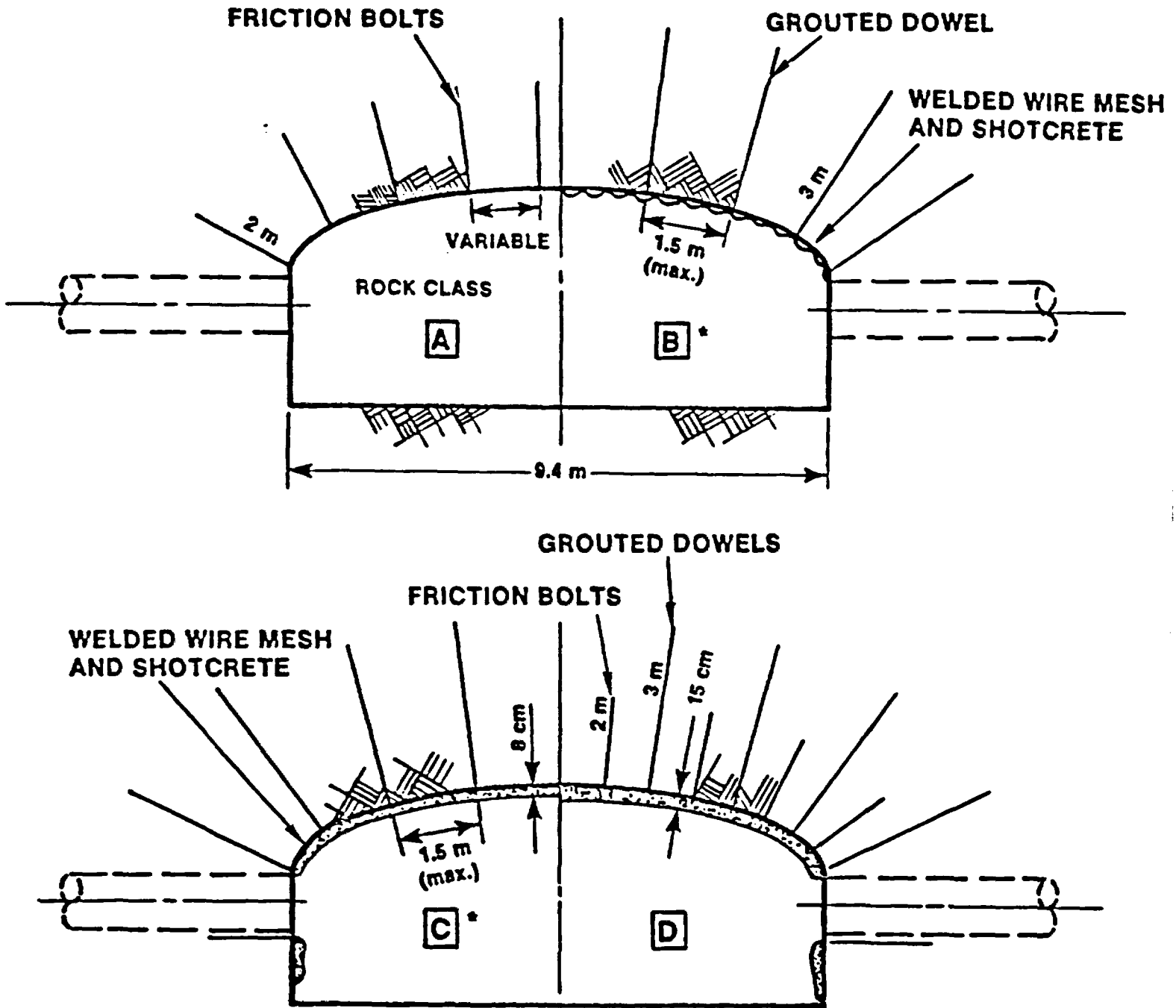


Figure 2-3. Typical Ground Supports for Horizontal Configuration

estimating support requirements on the NTS. The NTS requirement is that rock bolts and wire mesh can be used with a minimum of a 1.2-m spacing between the bolts, and the lengths of the bolts are a minimum of one-half the width of the opening.

The basic PBQ&D recommendation for repository Class B drifts was for seven grouted rock bolts, 3.0 m long and spaced in a 1.5- x 1.5-m pattern, with welded wire mesh. The recommended wire mesh was 9-gage wire welded in a 10.2- x 10.2-cm grid. Included in the recommendation was the provision that the rock bolts and mesh would be installed at the time of excavation. SNL made two changes to these recommendations. The first was that a woven wire (chain link) mesh would be used. The welded wire mesh was recommended because a better view of the rock surface would be available and the welded wire mesh could be used with shotcrete if necessary. Woven wire mesh, made from 11-gage steel and in a nominal 5- x 5-cm pattern, was readily available in rolls 2.4-m wide at G-Tunnel. The second change was that the rock bolt pattern was changed from 1.5 x 1.5 m to 1.5 x 1.2 m to accommodate the width of the woven wire mesh during installation. Neither of these changes was judged to threaten safety aspects in the mining. The final design shape and ground support pattern is shown in Figure 2-4.

Along with the ground support recommendations, PBQ&D recommended that alternate ground support systems be demonstrated. It was realized that the drift was too short to conclusively select one ground support method over another, but insight regarding any problems could be gained by using different ground support methods in welded tuff. The current practice of using resin-grouted rock bolts is quite suitable for ambient temperatures, but the rock bolts are susceptible to creep when subjected to heat, such as would occur in a repository setting. Therefore, nonresin-based grouts or other types of ground support, which have more promise for repository applications, were used in this investigation.

Two types of cementitious grouts were used (Report A). Sulfaset, a gypsum-based grout, was used in the two rows immediately following Station E (Round 8). Portland cement grouts were used for the next two

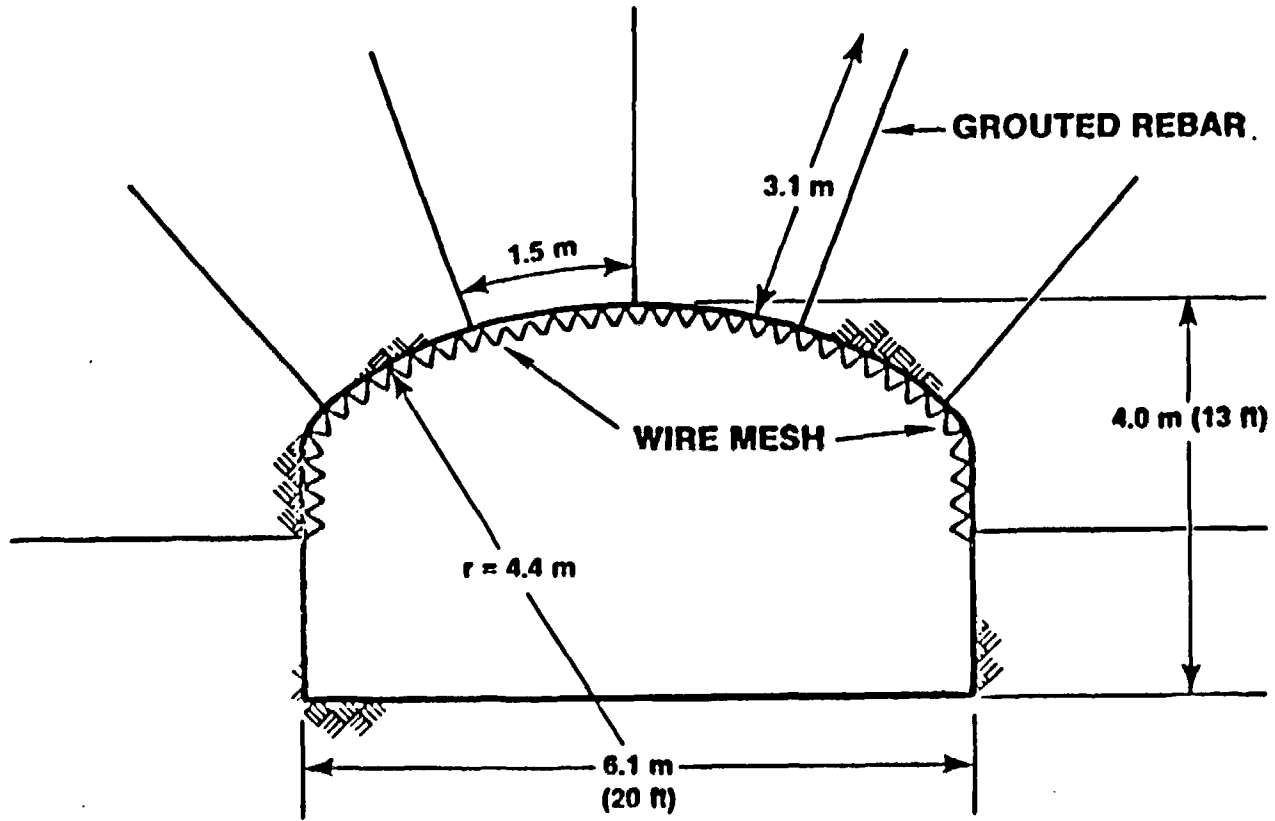


Figure 2-4. Final Ground Support for Demonstration Drift

rows of bolts (Round 9). The next two rows of holes (Round 10) were fitted with Swellex rock bolts. Swellex bolts are friction-type rock bolts that are inserted and expanded against the hole surface with water pressure.

The final ground support for the remainder of the drift (Rounds 11 and 12) was fibercrete, a steel fiber-reinforced shotcrete that was applied directly to the freshly mined surface in thicknesses ranging from 76 mm (3 in.) to 127 mm (5 in.). The fibercrete was sprayed on through a hand-held nozzle. Mixing of components was at the nozzle. The fibercrete used had approximately 1% fibers by weight.

#### 2.2.4 Ground Support Discussions

The resultant ground support effectiveness is discussed in light of the drift convergence results (Chapters 3 and 4). The focus here is on the overall adequacy of the ground support system from a qualitative standpoint.

The presence of the fault provided the most challenge to the ground support system. While the rock quality in the fault was not good, with one exception, the extent of the fault was not large enough to warrant a change in the rock bolt patterns. In the fault zone, the miners added two extra rock bolts in one area where the rock was more fractured.

Installation of rock bolts proved to be routine with the exception of one rock bolt grouted with Sulfaset. The borehole intersected a significant fracture, and over 0.38 m<sup>3</sup> (100 gal) of grout was pumped in. The surface indication of the fracture was later found (with some of the Sulfaset on the surfaces) approximately 4.6 m down the drift, after the mining face had advanced beyond the fracture. It might have been more difficult to grout the hole with a slower setting Portland-cement-based grout. The experience points to one of the problems associated with grouted rock bolts in a fractured rock, namely the possibility for fractures to carry the grout away from the rock bolt and require large quantities of grout and/or result in incomplete grouting of the full length

of the rock bolt. If rock bolt grouting is pursued further, Simpson et al. (1980) have shown how cement grout cartridges with encapsulated water can be used in fractured rock conditions, and these might be used in future investigations.

In summary, from a qualitative standpoint, the recommended ground support pattern appeared to be adequate for the welded tuff in G-Tunnel, and there were no apparent problems with using rock mass classification systems for defining initial ground support requirements in the welded tuff.

### 3.0 DRIFT CONVERGENCE BEHAVIOR

The drift convergence measurements and analyses are discussed in terms of drift convergence magnitudes and rates for the drift surface. These two quantities are affected by the original geologic processes, rock properties, in situ stresses, drift shape, other drifts, and groundwater pressure, although the latter is not a factor in G-Tunnel or at Yucca Mountain. Convergence measurements reflect the alteration of the stress field around the openings and exhibit variations caused by joint or block movements or shear zones and other variations. Drift convergence magnitudes and rates relate directly to support system displacement capacities, possible requirements for added drift maintenance, and/or requirements for possible redesign of the support systems for repository uses.

#### 3.1 Drift Convergence Magnitudes

For these discussions, drift convergence magnitude is taken as the full-drift convergence over the duration of the measurements. This term is used because of the difficulty of establishing a precise transition from the near-elastic response immediately after the mining to the smaller time-dependent responses that followed.

##### 3.1.1 Tape Extensometer Measurements

Figures 3-1 and 3-2 (Report B\*) provide the tape extensometer (TE) histories describing the overall vertical drift convergences. The figures show that the majority of the drift convergence phenomena occurred soon after the nearby rock was removed and the longer term contributions were relatively small.

Table 3-1 provides a summary of the maximum displacements at the measurement stations (Report B). The largest vertical displacements occurred at Stations D and E and the smallest at Station F. The largest

---

\*Zimmerman et al., in prep. b.

TABLE 3-1

SUMMARY OF MEASURED DRIFT CONVERGENCE MAGNITUDES\*

---

<u>Station</u>	<u>Tape Extensometer</u>	
	<u>Vertical</u> <u>(mm)</u>	<u>Horizontal</u> <u>(mm)</u>
A2	13.0	--
B	10.8	5.5
C	13.9	10.0
D	17.0	8.2
E	18.5	3.0
F	9.5	2.0
G	9.8	3.0

Multiple-Point Borehole Extensometer

<u>Station</u>	<u>Vertical</u>			<u>Horizontal</u>		
	<u>Roof</u> <u>(mm)</u>	<u>Floor</u> <u>(mm)</u>	<u>Total</u> <u>(mm)</u>	<u>South</u> <u>(mm)</u>	<u>North</u> <u>(mm)</u>	<u>Total</u> <u>(mm)</u>
C	2.5	5.5	8.0	2.4	0.3	2.7
E	2.0	4.0	6.0	-0.5	0.5	0

---

\*Convergence into drift is positive. Magnitudes indicate total time-independent convergence.

---

horizontal displacements occurred at Stations C and D and the smallest at Station F. Probable reasons for the variations in the displacements are discussed in Section 3.1.3, where the MPBX measurements are factored in.

3.1.2 Multiple-Point Borehole Extensometer Measurements

Figure 3-3 (Report B) shows the history of the vertical MPBX measurements for the surfaces of the roof, and floor gaps in data and variations,

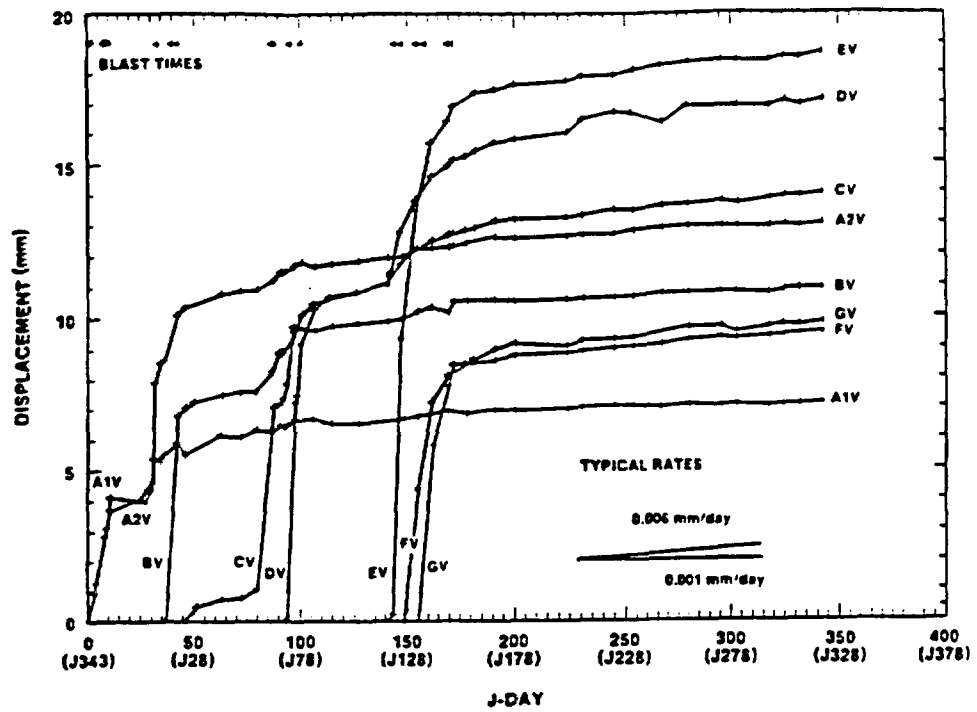


Figure 3-1. Summary of Vertical Tape Extensometer Data

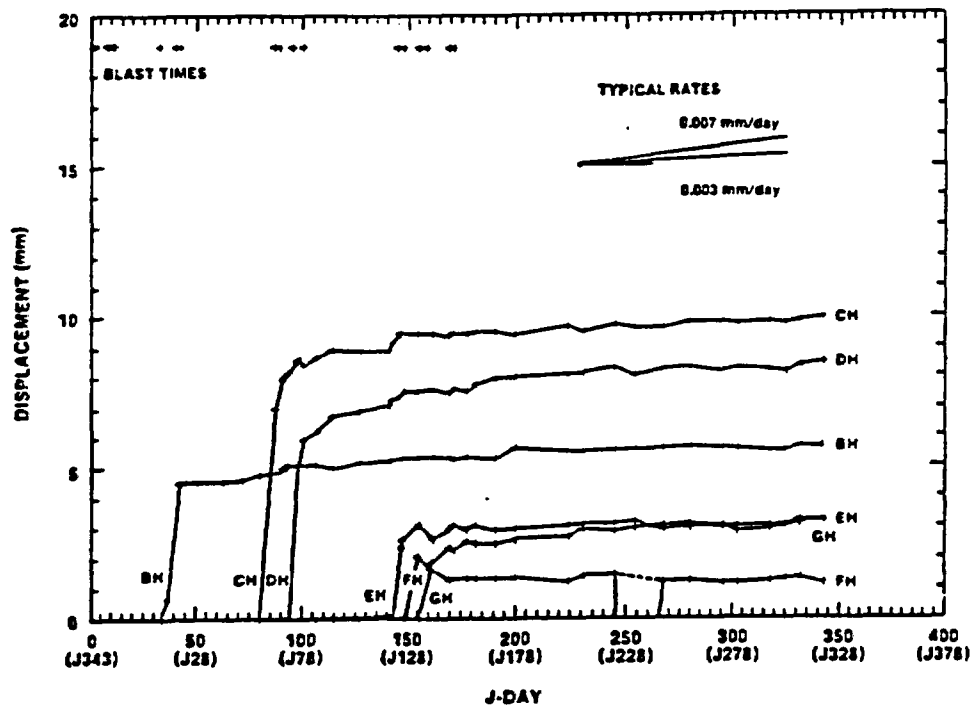


Figure 3-2. Summary of Horizontal Tape Extensometer Data

which are discussed in Report C.\* The MPBX collar displacements for the roof, relative to the deepest anchors in Figures 3-3a and 3-3b are summarized in Table 3-1. Table 3-1 also lists the corresponding floor displacements. Two trends are apparent: the floor displacements were noticeably larger, and the largest displacements occurred at Station C.

Figure 3-4 (Report B) shows the history of the horizontal drift surface MPBX measurements. Results are summarized in Table 3-1. The table shows that the largest range of displacements occurred between measurements on the left side. The range for displacements on the right side was relatively small.

### 3.1.3 Convergence Magnitude Discussions

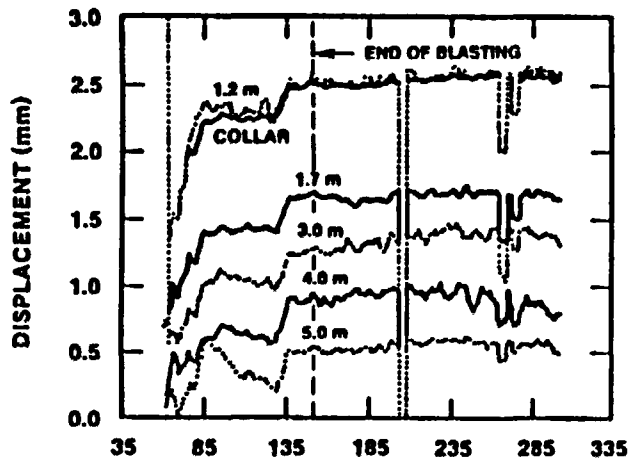
There are three evaluations that are directly applied to the surface-based convergence measurements. They are (1) interpretations of rock behavior through comparisons of TE and MPBX measurements, (2) comparisons of measurements with computer model outputs, and (3) comparisons of measurements with generic case history criteria.

#### 3.1.3.1 Comparisons of Tape Extensometer and Multiple-Point Borehole Extensometer Measurements

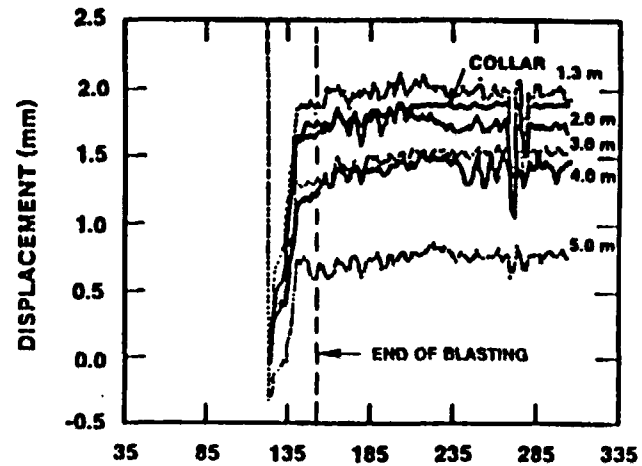
The magnitudes and differences in the TE and MPBX measurements in Table 3-1 can be used to explain and interpret the rock behavior. First, the factor of geometry, defining the regions of influence of the two measurement systems, needs to be considered. This factor relates to both vertical and horizontal measurements. The MPBX displacements were limited to displacement changes within a 15-m interval, while the TE measurements summarized the drift displacements of the entire volume of rock being affected by the excavation. On a smaller scale, the TE anchors, located

---

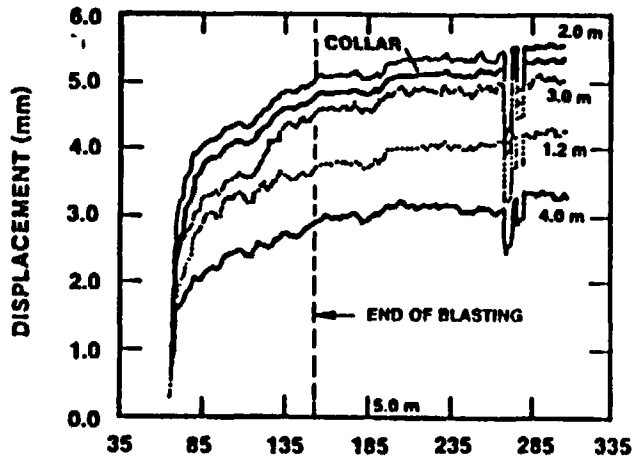
\*Zimmerman et al., in prep. c.



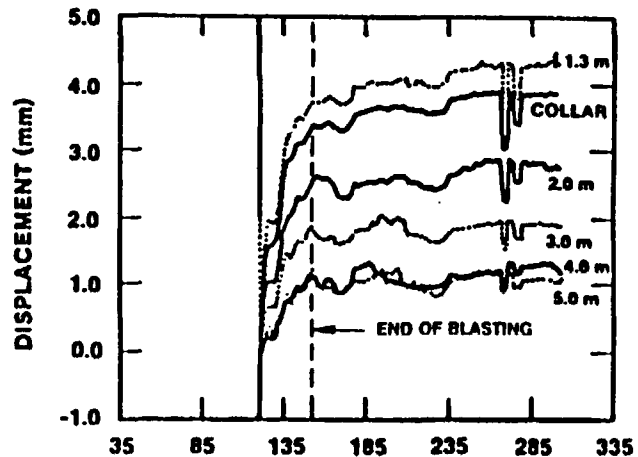
J-DAY  
(a) STATION C--ROOF (C3)



J-DAY  
(b) STATION E--ROOF (E3)

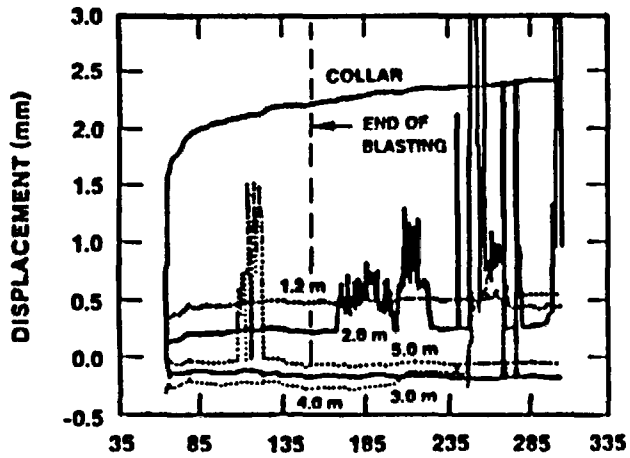


J-DAY  
(c) STATION C--FLOOR (C6)

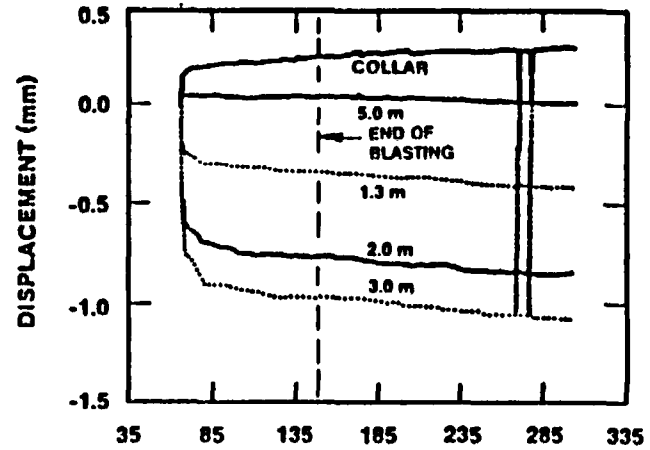


J-DAY  
(d) STATION E--FLOOR (E6)

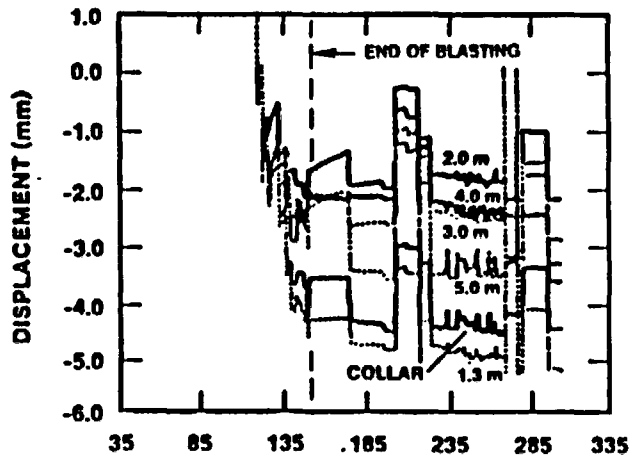
Figure 3-3. Vertical Multiple-Point Borehole Extensometer Displacement Histories at Stations C and E (Bottom Anchor Relative)



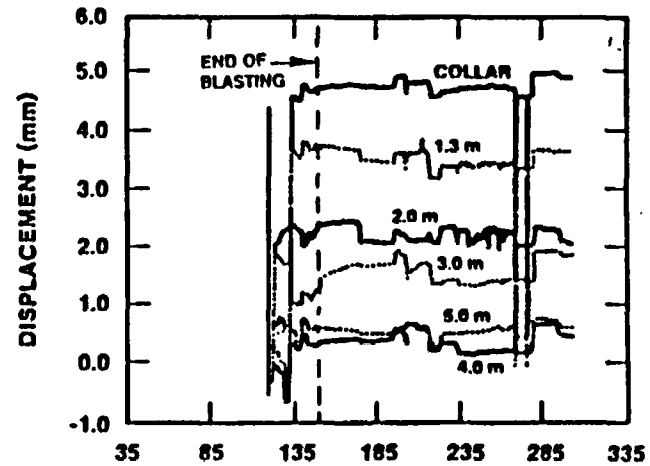
(a) STATION C--LEFT (C1-GEOKON)



(b) STATION C--RIGHT (C5-GEOKON)



(c) STATION E--LEFT (E1-SINCO/TERRAMETRICS)



(d) STATION E--RIGHT (E5-SINCO/TERRAMETRICS)

Figure 3-4. Horizontal Multiple-Point Borehole Extensometer Displacement Histories at Stations C and E (Bottom Anchor Relative)

near the surface, would logically indicate slightly more rod movement than the collars of the MPBXs, which were recessed and grouted in.

The possibilities for influences based on geological characteristics are quite broad and are discussed in terms of (1) stratigraphic effects (primarily rubble zone) and (2) geologic structure (fault and related fractures). The presence of the rubble zone (Figure 1-2) had the potential to affect the TE-based vertical convergence measurements the most (Figures 3-1 and 3-3). Possible deformation of the rubble zone, which was assumed to be less stiff than the welded tuff, could influence the TE measurements because the rubble zone was included in the volume of rock contributing to the TE anchor deformations; this was not the case for all of the MPBX measurements, however. The rubble zone may have affected the collar measurements in the floor at Station C, because the collar was in the zone. At Station E, the floor-mounted MPBX collar was in the vitrophyre (Report A).

The fault, shown in Figure 1-1, went through the Demonstration Drift between Stations C and D. In situ inspections revealed that the roof-related fractures appeared to be in the rock on the higher side of the fault in the vicinity of Stations D and E, where there were possible extension zones in the rock. It is reasoned that the rock between Stations C and E was affected in some way by the fault. For example, Figure 3-1 shows that the largest TE displacements occurred at Stations D and E. The roof anchors at these convergence stations were in rock that was more fractured than other convergence stations based on visual observations, and this additional fracturing may have contributed to the larger TE displacements. The vertical MPBX measurement at Station E (Figure 3-3) would be expected to support this hypothesis, but the MPBX collar at that station was observed to be in rock that was separated from the TE anchor, and it is likely that the MPBX measurements were isolated from the larger deformations recorded by the TE. Also, the MPBX protective measures may have influenced the rock around the anchor and recess. The recess was blasted to a depth of approximately 0.5 m, and then the cover plate was rock bolted into the rock. It is possible that the blasting operation may have

influenced the rock around the TE anchor, or the short rock bolts may have reduced the MPBX collar displacement somewhat.

The geologic factor is assumed to be the primary reason for the differences in the TE and MPBX horizontal measurements. The horizontal TE convergence at Station C was 10 mm, while it was nearly 3 mm at Station E. The intersection of the fault and the drift was closest to Station C. It is interesting that the largest horizontal convergence magnitudes were at the MPBX installations nearest to the intersection of the fault with the Demonstration Drift (C-left and E-right). This suggests that there might have been shear zone disturbances in those regions as a result of the excavation.

#### 3.1.3.2 Comparisons of Measured Convergence and Model Predictions

A comparison of measurement results (Table 3-1) with linear-elastic model predictions (Table 3-2) provides information pertinent to describing the rock behavior and to determining model limitations. These comparisons are limited to the drift surface behavior. The linear-elastic model is briefly described in Appendix A.

The first comparison is between the model predictions and the TE measurements taken in the vertical direction. To do this properly, there are necessary qualifications. First, the computer predictions were a two-dimensional approximation that most closely models the full excavation of a very long drift, while the TE measurements were initiated after some excavation. To compare predictions and measurements, it is necessary to account for the partial convergence that occurs before the initial measurements. Brady and Brown (1985) published the displacement profile for the excavation of a circular tunnel in a hydrostatic stress field using linear elasticity. They showed that the displacement at the face of an excavation is approximately 30% of the total convergence for that location. Convergences in the excavated region were expressed as a function of the ratio of the distance from the drift face ( $x$ ) to tunnel radius ( $r_i$ ). If the tunnel radius were assumed to be 3 m, and the distance from the face to

the furthest anchor was 1 m, then the  $x/r_i$  value would be 0.33, and approximately 65% of the convergence would have occurred at the time of installation of anchors for the extensometers and the initiation of measurements. If the radius were assumed to be the 4.4 m used to establish the drift shape (Figure 2-4), then a  $x/r_i$  value of 0.23 would predict an anchor initial convergence value of approximately 60%. For the purposes of comparing model predictions and field measurements, the model predictions for TE convergence will be taken as 40% of the total convergence calculated. This means that the total predicted vertical displacement of 12.1 mm from Table 3-2 would be reduced to 4.8 mm.

The second qualification deals with the elastic constants used in the numerical model. Table A-1 lists recommended values for the modulus of deformation and Poisson's ratio. The modulus values are referenced to Zimmerman and Finley (1987), where the modulus of deformation was taken as a factor ( $K = 0.615$ ) x intact rock value. This value was taken from the heated block experiment, where effects of in situ stresses were factored into the measurements (Zimmerman et al., 1986). The modulus of deformation is highly dependent on the size of the unstressed apertures, the frequency and orientation of fractures, and the stress state, and accurate generalizations are difficult. Subsequent measurements in G-Tunnel Pressurized Slot Testing have suggested that the modulus of deformation "K" factor can be reduced to as low as 0.5 (Zimmerman et al., in prep. d). If this were the case, the predicted convergence could be increased by the ratio  $0.615/0.5 = 1.23$ . Because of the limited amount of data available, it is perhaps prudent to leave the predicted vertical convergence at 4.8 mm and provide conservative estimates for the comparisons.

In making measurement/model result comparisons, it is useful to select a single value to be representative of the unfaulted welded tuff. The measured TE displacements ranged from 9 to 19 mm in Table 3-1. Discussion in Section 3.1.3.1 showed that the maximum displacements at Stations D and E were probably influenced by the fault zone. The minimum displacements at Stations F and G could have been influenced by the drift end effects. If these displacements were discounted, the average of the three remaining

TABLE 3-2

SUMMARY OF PREDICTED DRIFT CONVERGENCE MAGNITUDES\*

<u>Model Representation</u>	<u>Direction</u>	<u>Descriptive Term</u>	<u>Quantity (mm)</u>
Total Convergence	Vertical	Roof	4.7
		Floor	7.4
	Horizontal	South	0.6
		North	1.0
MPBX (surface relative to a 15-m depth)	Vertical	Roof	2.2
		Floor	6.5
	Horizontal	South	0.1
		North	0.3

\*Full convergence for drift excavation using linear-elastic model.

displacements would be 12.6 mm. The average of all seven displacements is 13.2 mm. A reasonable single value appears to be 13 mm.

A quantity useful for later comparisons is the ratio of the measured displacement to the predicted elastic displacement. Cording (1974) used ratios of measured displacements to predicted continuum displacements in evaluating stability criteria. The ratio is useful because it provides an estimate of the displacements the rock mass would undergo if movements were minimized. Using the simplified single value for TE convergence for this study, the ratio of measured displacements to predicted elastic displacements would be  $13/4.8 = 2.7$ .

A second comparison is between the elastic model result and the MPBX measurements in the vertical direction. The computed convergence was 8.7 mm; thus, the 40% representation for prior excavation effects would be 3.5 mm. The corresponding sum of the MPBX measurements ranged from 8.0 mm

at Station C to 6.0 mm at Station E. An average would be 7.0 mm. The ratio of the measured to the computed can be represented as  $7.0/3.5 = 2.0$ .

These two comparisons of measured to predicted values for vertical measurements indicate that the measured displacements were approximately 2.0 to 2.7 times as large as the predicted. The similarities in the results of the two comparisons suggest that the elastic model predictions are uniformly low. Possible reasons for these differences including the effects of modulus of deformation differences are addressed in Chapter 4 where the localized effects of the measurements and rock are considered. Differences in the two magnitudes can be partially attributed to the geometric and geologic factors discussed earlier in this section.

A final comparison is of the horizontal MPBX measurements with predicted values. Table 3-1 shows that the total MPBX collar-bottom anchor relative measurements ranged from 2.7 mm at Station C to approximately zero at Station E. The total predicted convergence displacements would be  $(0.1 + 0.3)0.4 = 0.16$ . Discussions in Chapter 4 show that geologic effects are the most likely causes for the differences.

### 3.1.3.3 Comparisons of Measurements With Case History Criteria

Cording (1974) provided results from comparisons of measured and predicted displacements for 13 large rock-bolted underground chambers. In situ values of the modulus of deformation were used in the elastic calculations. Most of the chambers were for underground power stations. Where extensive rock loosening did not take place, displacements ranged from 1 to 2 times the predicted elastic displacement. Movement and loosening along joints were usually indicated when the observed displacements were more than 3 times the elastic displacements. In many cases, where the displacements exceeded the computed elastic displacements by a factor of 5 or 10, the excavation and support procedures required modifications.

If Cording's criteria for underground chambers were applied, the comparison would suggest that some rock loosening may have occurred. Cording also pointed out that the magnitudes of displacements should not be the sole criterion for evaluating modification of supports. Other considerations should include rates of displacement, displacement capacities, rock volume considerations, measured displacements in well-supported sections, and visual observations.

Bieniawski and Maschek (1975) provided a synthesis of other excavation measurements and have expressed them in ranges that are relevant to stability considerations. They summarized results of evaluations of underground behavior, including significant input from the Cording (1974) study, and suggested ranges of displacement magnitudes that are relevant to stability considerations. They observed that drift convergence magnitudes on the order of 12 to 75 mm are considered large and support displacement capacities should be considered.

### 3.2 Drift Convergence Rates

#### 3.2.1 Tape Extensometer Measurements

Drift convergence rates for the vertical measurements can be obtained using data presented in Figures 3-1 and 3-2. The last 10 points were linearly regressed to establish TE convergence rates, and the results are summarized in Table 3-3.

#### 3.2.2 Multiple-Point Borehole Extensometer Measurements

Figure 3-3 provides the reference data for the vertical MPBX measurements. Slopes for data trends were visually established over the last 100 days of measurements because of the large number of data collected. Results are summarized in Table 3-3.

TABLE 3-3

SUMMARY OF MEASURED DRIFT CONVERGENCE RATES\*

---

<u>Station</u>	<u>Tape Extensometer</u>	
	<u>Vertical</u> <u>(mm/day)</u>	<u>Horizontal</u> <u>(mm/day)</u>
A1	0.0014	--
A2	0.0045	--
B	0.0033	0.0010
C	0.0061	0.0037
D	0.0120	0.0023
E	0.0092	-0.0004
F	0.0062	-0.0016
G	0.0068	0.0049

Multiple-Point Borehole Extensometer

<u>Station</u>	<u>Vertical</u>		<u>Horizontal</u>	
	<u>Roof</u> <u>(mm/day)</u>	<u>Floor</u> <u>(mm/day)</u>	<u>South</u> <u>(mm/day)</u>	<u>North</u> <u>(mm/day)</u>
C	0.0004	0.0017	0.0008	0.0002
E	0.0003	0.0007	0.0000	0.0008

---

\*Convergence into the drift is assumed to be positive

---

3.2.3 Convergence Rate Discussions

Table 3-3 shows that the largest drift convergence rates occurred in the floor. This is commonly called floor heave. The floor was unsupported, unlike the roof and upper side walls. The floor of the Demonstration Drift is very near (within 1.5 m) the underlying nonwelded tuff unit, a material low in strength and stiffness (Zimmerman and Finley, 1987). The combination of the relatively low strength and stiffness and the lack of support is assumed to contribute to the larger displacements that occur. Floor heave is sometimes observed in nonwelded tuffs on the Nevada Test Site (NTS). In the Small-Diameter Heater Alcove in nonwelded tuff in G-Tunnel, floor displacements of approximately 8.0 mm were observed to follow the alcove excavation (Zimmerman and Finley, 1987). Floor heave

stabilizes with time in G-Tunnel and is not considered as a significant factor over a long period of time.

An additional factor that could have influenced the floor behavior is that water was injected into the rock as part of the HQ measurements. Water was injected in the rock forming the floor at Stations B, D, and F. The water could have influenced the floor heave process, either by direct pressure in the stratified tuffs or chemical action with the uncharacterized clay in the rubble zone near Stations C and D.

Bieniawski and Maschek (1975) reported ranges for drift convergence rates based on case histories. They reported that rates on the order of 0.001 mm/day would indicate stable conditions and that rates of 0.05 mm/day would be considered high for wide chambers. Rates over 1.0 mm/day were considered excessive and would call for additional support measures. It is not clear from Bieniawski and Maschek's paper whether they considered the drift convergence rates for the total drift or for drift surfaces. Cording (1974) considered surface displacements and it is assumed that was the intent in the Bieniawski and Maschek discussion. Roof displacement rates are used for comparison purposes in this report. The largest roof convergence rate of 0.0004 mm/day is low according to the aforementioned criteria.

### 3.3 Support Displacement Capacities

Bieniawski and Maschek (1975) discussed rock displacements and support displacement capacities. Displacements should not exceed the capacity of the rock mass to maintain its strength and coherence because rock strength along joints decreases with joint displacements. The ground support was divided into four classes by PBQ&D (Report A), ranging from friction rock bolts to a composite of grouted dowels, welded wire mesh, and fibercrete. The friction-type rock bolt would have a relatively large displacement capacity, while the fibercrete would be considered to have a low displacement capacity. For example, Bieniawski and Maschek reported that tensioned rock bolts (stiffer than friction bolts) broke when displacements approached 50 mm. On the other hand, shotcrete (similar to fibercrete) was

observed to crack in tunnels when the differential movement between rock blocks exceeded 2.5 mm. Cracking without noticeable distortion in shotcrete does not necessarily mean failure of the ground support system, only that a load is being applied and the system is responding.

Distinction is made between tensioned rock bolts and grouted rock bolts. A tensioned rock bolt is anchored at the end, and there is a tension force between the base plate and the anchor. For a tensioned rock bolt, joints and fissures in the rock between the end of the bolt and the base plate can open up, and the load is distributed over the unsupported length of the bolt. Tensioned rock bolts have relatively high strain capacities. A grouted rock bolt has a bonding agent between the rock bolt and the rock, and shear is transferred along the length of the bolt; the base plate is essentially ineffective. Pells (1974) discussed the differences in behavior of tensioned and grouted rock bolts. For the grouted rock bolt, it is not certain that the full length of the rock bolt is loaded, for if the bond between the grout and the rock bolt is strong, all the joint-induced strain can be confined to the small length of the bolt in the immediate vicinity of the joint. With high strains concentrated in short rock bolt lengths, failure of rock bolts can occur with relatively small overall rock bolt strains.

Pells performed tests on fully bonded rock bolts under simulated field loading conditions. He developed a test arrangement such that the effect of a joint opening up near the center of a 1-m rock bolt could be studied. He showed that 20- to 22-mm-dia rebars grouted with resins and cements had maximum joint openings ranging from 38 to 100 mm. Maximum forces for all tests exceeded 200 kN, but loads at the maximum displacements ranged from 40 to 274 kN. The largest force corresponded to the smallest joint displacement. He noted that in all cases the peak load had been reached before the joint had opened 50 mm. In the case of the cement grouts, the bolt always sheared free of its bond, while with the resin grouting, the bond strength was sufficient to cause failure of the steel. It was clear in the cases where the steel failed that the inelastic strain was limited to a short length of rock bolt on either side of the opening joint. In all

cases, the bond between the grout and the rock was adequate. Pells concluded that the grouted rebar rock bolt developed good resistance to rock movement, but it does not have a large displacement capacity.

This brief review of support displacement capacities provides information that can be used for a support displacement capacity analysis. The MPBX displacements in the roof provide the best analog for the rock mass displacements that would affect the rock bolts. The largest roof convergence magnitude was 2.4 mm, and the largest roof convergence rate was 0.0004 mm/day. If the maximum convergence, a conservative roof convergence rate of 0.001 mm/day, and a drift operational period of 80 yr were used, the total predicted displacement would be  $2.4 + 29.2 = 31.6$  mm, a value within the smallest joint displacement (38 mm) reported by Pells. Within this rather simple calculation, it is apparent that the grouted rock bolt technique as used in the Demonstration Drift is adequate for short-term applications under ambient temperatures but that it might be marginal for long-term applications. Thermal stresses could complicate the situation, but analysis of that aspect is beyond the scope of this report.

#### 3.4 Drift Convergence Summary

The drift convergence data discussed in this chapter have been organized into presentations of drift convergence magnitudes, convergence rates, and support displacement capacities. Displacement magnitudes were compared with predicted elastic model outputs and available case history information. Results indicated that some rock loosening might have occurred. Evaluations of roof convergence rates and support displacement capacities indicated that the grouted rock bolt system used in the Demonstration Drift would be adequate for short-term applications under ambient temperatures such as might be used for the ES. Repository designers may wish to look into displacement capacities for longer term considerations.

## 4.0 RELAXED ZONE AND RELATED ROCK MASS EVALUATIONS

This chapter presents evaluations of the effects of the excavations on the rock surrounding the opening. The relaxed zone is defined and described, and then the Hydraulic Quotient (HQ) and MPBX measurements used to define the zone are discussed. The Hydraulic Quotient (HQ) measurements are also used to provide estimates of the hydraulic properties of the fractured welded tuff in order to extend the data base for welded tuffs.

### 4.1 Relaxed Zone Description

The relaxed zone is taken as a special component of the more general disturbed zone. The NRC (1981) defines the disturbed zone as

that portion of the controlled area whose physical or chemical properties have changed as a result of underground facility construction or from heat generated by the emplaced radioactive wastes such that the resultant change of properties may have a significant effect on the performance of the geologic repository.

For repository sealing purposes, Kelsall et al. (1982) have described the disturbed zone as the zone around the perimeter of an excavation that is influenced by (1) stress redistribution, (2) damage by the excavation process, and (3) weathering and rock/groundwater interaction.

The relaxed zone in this document is taken to be the zone around the perimeter of an excavation where there are rock property changes as a result of blasting and rock removal. The main difference between the definition of the relaxed zone and that of the disturbed zone is that the relaxed zone is formed with and immediately after the excavation, while the disturbed zone can have time-dependent influences. The stress redistribution and blast damage effects are introduced in the following two subsections.

#### 4.1.1 Stress Redistributions

The relaxed zone as defined includes the first two of the three factors listed by Kelsall et al. (1982). In the first case, the main features contributing to the formation of the relaxed zone are (1) the stresses normal to the surface of the opening that are relieved and (2) stresses tangential to the opening, which may be increased as a result of stress concentrations or decreased according to the rock mass responses. Stress redistributions can lead to the formation of special zones around underground drifts, which can be summarized as (Cording et al., 1971)

- (1) a gravity zone--roof stresses are redistributed, and loosening or tensile regions can form that allow gravity falls in unsupported blocky-jointed rock;
- (2) a shear zone--unfavorable orientations of major joint sets and shear zones are present that can cause internal rock movements, which may threaten stabilities; and
- (3) a slabbing zone--high compression or unsupported surfaces can form, leading to minor spalling or separations of slabs of rock. This is sometimes called wall slabbing, but it can also be a form of floor heave if compressive stresses are present.

On a broader scale, there are five factors that are identified as major contributors to stress redistributions around excavated openings. This listing is a synthesis of factors commonly found in the literature. The factors are

- the size of the opening relative to the fracture spacings and orientations,
- the shape of the opening,
- the strength of the intact rock,

- the in situ stress field, and
- possible ground support interaction.

#### 4.1.2 Blast Damage

The second of the major factors contributing to the formation of the relaxed zone is often referred to as blast damage. There are generally three zones that are used to describe blast damage (Worsey, 1985; Case and Kelsall, 1987; Brady and Brown, 1985):

- A crushing zone--expansion of high-pressure gases results in formation of a dynamic stress wave that causes local crushing of the borehole and limited radial cracking. Siskind et al. (1974) point out that the thickness of the crushed zone can be on the order of the radius of the borehole. It can be larger if the blasting intent is to fracture the rock rather than to minimize blast damage.
- A highly fractured zone--expansion of gases that results in development of radial cracks. Brady and Brown report that this zone is on the order of four to six times the radius of the borehole. The wave motion in a radially compressive zone may cause cracks to extend to approximately nine times the radius of the hole.
- A lightly fractured zone--passage of original or reflected compression waves that result in developments of limited tensile fractures. Wave reflections may be a result of open fractures or void spaces. During the transmission of the waves, longer fractures may be initiated at the radial cracks. When the geometry is favorable, the fractures develop in planes parallel to the perimeter leading to a definition of a controlled perimeter. The radial fracturing should be expected to extend along the controlled plane to a minimum of one-half the borehole spacing. In the WTM,

the perimeter spacing was 0.61 m; thus, the desirable extent of fracture growth should be about 0.3 m.

A notable study that attempts to distinguish blast damage from stress redistribution effects was conducted by Worsey (1985). He reported on blast damage investigations in dolomites and indicated that the extent of actual blast damage (assumed to include the highly and lightly fractured components) for control blasting conditions may be within 1 m.

#### 4.1.3 Other Relaxed Zone Determinations

Relaxed zone estimates can be made from limited data other than permeability or MPBX data that are available. Kelsall et al. (1982) reported that a disturbed (relaxed) zone thickness typically is in the range of 0.3 to 0.7 times the excavation radius. In a case history, Scott et al. (1968) reported on the Straight Creek Tunnel pilot bore in Colorado. The 4-m-dia bore was driven through granite, gneiss, schist, and magmatite, which were extensively faulted, sheared, and locally altered. Seismic reflection measurements showed a low-velocity layer adjacent to the tunnel walls, which varied in thickness from less than 1 m in more competent sections to about 5 m in severely fractured sections of rock. The authors judged the blast damage effects to be within the first "few feet" in the rock, and the remainder of the disturbance was a result of stress redistributions. The same study included results of electrical resistivity measurements and reported that the relaxed zone appeared to range from 0.3 to 3 m. In addition, Carroll and Scott (1966) reported on seismic investigation results of mining in granite drifts on the NTS. This report suggested that the blast-damage effects were limited to 1.2 m and that there were relaxed zone disturbances to the rock at distances up to 2.4 m.

The relaxed zone can be viewed from another perspective, that of effective rock bolt lengths. Cording et al. (1971) studied applications of rock bolts to underground caverns of various sizes. They found that rock bolt lengths for arched crowns typically ranged from 0.2 to 0.4 times the

maximum width. They noted that the rock bolt length should be longer for flat surfaces. Also, they found that rock bolt lengths on the planar side-walls nominally ranged from 0.1 to 0.5 times the height. The smaller value is commonly used to support loosened skin, and the larger value is used when there are deep-seated joints or shear planes. The report mentioned that some underground caverns have needed rock bolts having lengths on the order of the width dimension in cases where large shear planes developed.

In summary, the limited information on the definition of the relaxed zone under controlled-blasting conditions suggests that the relaxed zone can be expected to be composed of the blast-damaged zone and the stress relief zone. The blast-damaged zone is small when controlled blasting is used but can be up to 1 m in dimension, and the stress relief zone is most likely on the order of 2 to 3 m or possibly some fraction of a major dimension describing an excavation.

#### 4.2 Relaxed Zone Evaluations Using Hydraulic Quotient Measurements

The development of the relaxed zone in the WTM was monitored by two methods: (1) borehole injection (BI) measurements in boreholes and (2) MPBX measurements. These two were selected because of technical feasibility, practicality for G-Tunnel operations, and ability to incorporate measurements into other evaluations.

##### 4.2.1 Borehole Injection Testing Background

Technical criteria developed by the NRC (10 CFR 60, 1981) for the disposal of high-level radioactive wastes in geologic repositories call for minimizing the development of preferential pathways for radionuclide migrations. Conceptually, air or water can flow through existing fractures in the rock mass; thus, enhanced flow characteristics near underground openings are undesirable. Sequential BI measurements in the rock mass is the most common method for monitoring rock permeability changes (Kelsall et al., 1982). This is the method selected for G-Tunnel. The new feature

of this WTM series is to use BI measurements before and after the mining process so that the changes caused by the developments in the relaxed zone can be evaluated.

Two previous investigations form the nucleus of baseline experience for these measurements. Miller et al. (1974) performed air injection measurements in lightly fractured nonwelded tuffs in G-Tunnel. They sealed off successive 0.3-m intervals of boreholes up to 2.7 m deep and injected air at a nominal 172-kPa pressure in each interval. Seventeen radial boreholes were drilled from the inside of a drift, which was 3.0 m in diameter. Flow rates varied up to 283 m<sup>3</sup>/day (10<sup>4</sup> ft<sup>3</sup>/day). At least 90% of the measured flow rates greater than 17 m<sup>3</sup>/day were encountered in the first 1.7 m of the surface of the drift. They assumed that these high flow rates were associated with newly developed fractures, which would form in the wall slabbing zone.

Montazer et al. (1982) studied the spatial distribution of permeability within a 5-m-thick envelope around a room (3 m high and 5 m wide) in a fractured metamorphic rock. Air injection tests were used to identify and characterize conductive fractures around an existing opening. They found that the blast zone extended to approximately 0.5 m and that the effects of stress redistributions extended to a depth of approximately 3.5 m.

The method used here was discussed in Report A.\* The BI method consists of injecting matter into a packed interval and measuring the ratio of the flow rate to the injection pressure, which is called the HQ. The hydraulic injection method was selected over the air injection method because of availability of equipment in G-Tunnel and experience with the method (Zimmerman and Vollendorf, 1982). The air permeability testing at the Colorado School of Mines typically took 110 min, whereas hydraulic testing could be accomplished in 15 to 20 min per interval. Further, the HQ can be related to the cube of the aperture (see Equation 3-1 in Report B),

---

\*Zimmerman et al., in prep. a.

thus, it is highly sensitive to measuring changes in the apertures caused by relaxation effects.

The water injection method is not without limitations that must be considered in the overall evaluation. These limitations and assumptions are summarized as follows:

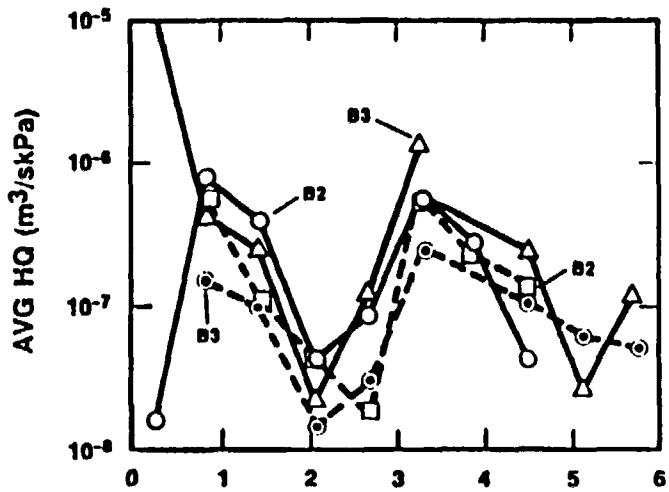
- There was no control for development of new fractures.
- There was no guaranteed leakage control.
- There was a constant hydraulic gradient in the rock.
- There was a constant temperature.
- The packer pressure had no effect on the fracture apertures.
- Steady state injections were achieved.

#### 4.2.2 Hydraulic Quotient Measurements

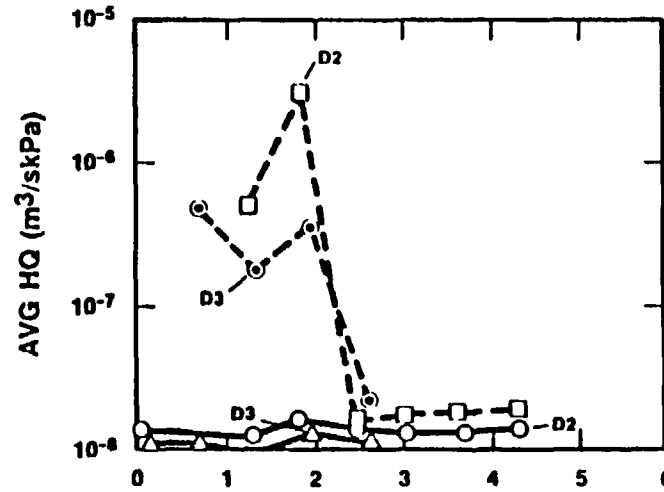
The basic relationships used in the HQ determinations were discussed in Report B.\* The HQ is a quantity that allows data from hydraulic pumping tests to be presented and analyzed. The focus in these relaxed zone evaluations is on the welded tuff in the roof of the Demonstration Drift. It is helpful to replot the HQ quantities. Figure 4-1 shows results from the six boreholes in three plots. The figure is plotted using the log of the HQ to better display all the data. The figure shows the premining value for each borehole nearest the surface so that initial trends are available. The postmining values from the first interval that could be measured beyond the surface are shown. The gap in the data for Borehole D3 was discussed in Report B.

---

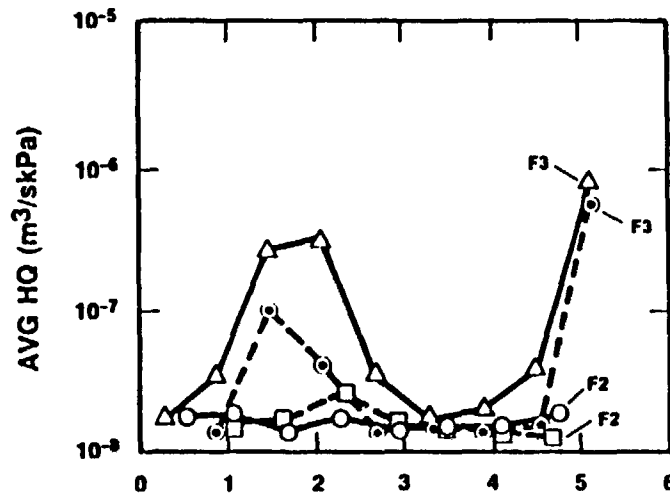
\*Zimmerman et al., in prep. b.



(a) BOREHOLES B2 AND B3



(b) BOREHOLES D2 AND D3



(c) BOREHOLES F2 AND F3

— = PREEXCAVATION  
 - - - = POSTEXCAVATION

Figure 4-1. Plots of Pre- and Postmining HQ Quantities for Welded Tuff Above Demonstration Drift

Before discussing Figure 4-1, it is helpful to locate the regions of HQ measurements. HQ measurements in the boreholes along the #2 line (Figure 1-2) intersected the Demonstration Drift near the center of the drift. Boreholes along the #3 line intersected the drift near the arch spring line on the right side.

Figure 4-1 shows two interesting trends. First, the figure shows that there were probably dominant preexisting fracture zones in three of the boreholes (B2, B3, and F3), and second, that there were probably significant relaxation zone developments in Boreholes D2 and D3 and to some extent Borehole F3.

Figure 4-1a suggests preexisting fractures (high premining HQ) near the surface and at a depth of approximately 3.0 m. In addition, the figure suggests that the trend was for slight closure of the fractures because of the reduction of the postmining HQ quantities. Figure 4-1b shows that HQ quantities increased significantly in Boreholes D2 and D3. The measurements were taken in the fault zone, and the data suggest a general loosening of the rock up to a distance of 2.5 m from the surface. The loosening appears to occur in the tensile zone that can be formed above the drift (Appendix A). The amount of loosening is estimated in Section 4.5. Finally, Figure 4-1c suggests that there were fractures between depths of 1.5 and 3.0 m in Borehole F3. The fractures appeared to tighten as a result of the mining. There was another fracture at a depth of 5.0 m that apparently was slightly, if at all, affected by the excavation. Borehole F2 was reasonably tight and remained that way. The boreholes at Station F could have been influenced by drift end effects.

In summary, within the limitations and assumptions listed in Section 4.2.1, the data presented in Figure 4-1 show that there were apparent excavation effects, which were most evident in the fault zone, Station D. At this station, the measurements indicated that the rock loosened up to a distance of 2.5 m. Measurements at the other stations indicated that there was a tendency for fracture closing because of the stress redistributions associated with the excavation process.

Borehole mappings were intentionally not incorporated in the HQ measurements and evaluations. Past experience (Zimmerman and Vollendorf, 1982) has shown that borescope investigations of welded tuff boreholes are difficult to interpret. Borescope investigations, either visual or with videotape, were considered in the planning of the HQ measurements, and the decision was made to attempt to develop a method that would be free of this encumbrance. Core logging was also considered, but experiences with coring in the heterogeneous rock have shown that natural fractures and drilling-induced fractures are hard to distinguish, and core logs provided only general information. Thus, the approach was to use BI alone for these evaluations. The results suggest that the pre- and postmining BI testing method can be useful in detecting relaxed zone developments in highly fractured zones without the mapping exercises.

#### 4.3 Relaxed Zone Evaluations Using Multiple-Point Borehole Extensometer Measurements

##### 4.3.1 Multiple-Point Borehole Extensometer Measurement Background

MPBXs were used as the second method to estimate relaxation effects. They were used primarily to document the rock mass behavior and provide input to drift surface convergence analyses. They were used here as a secondary method for evaluating the relaxed zone. There have been a limited number of studies where MPBXs have been used for this purpose. The more notable are by Cording et al. (1971), Benson et al. (1970), and Scott et al. (1968).

Cording et al. made comparisons between measured displacements and elastic theory predictions for caverns (up to 30 m in diameter) constructed in nonwelded tuffs. With the MPBXs, they found that there was a low-modulus loosened zone about 1 to 2 m thick. Other measurements indicated a shallow slabbing zone that extended several meters into the rock mass and some deep-seated movements along joints that occurred some 10 m from the surface.

Benson et al. performed plate-loading tests on gneiss. The plate-loading results were strongly affected by the compressibility of the blast-damaged rock around the underground openings. The rock quality was measured by computing the modulus of deformation for specific intervals between anchors of MPBXs. The results ranged from 3.5 MPa within a depth of 0.3 m to an upper value of 48 MPa further out in the rock mass. The cyclic measurements showed that there were no inelastic responses beyond a depth of 1 m.

Scott et al. installed extensometers in the pilot bore for the purpose of defining a tension zone above the Straight Creek Tunnel. The height of the tension zone was defined as the transition point between zones of compression and tension in the rock above the bore. Rock within the tension zone was observed to move toward the excavation, while rock outside the tension zone was observed to move away from the excavation.

The approach used in the WTM measurements was to install the MPBXs near the face and then monitor the convergence as the drift was extended. It was hoped that total convergence could be compared with elastic predictions to delineate the relaxed zone developments.

There were some limitations to the use of MPBXs for relaxed zone determinations. The more notable ones are that

- MPBXs were insensitive to changes within the first 1.0 to 1.5 m of the surface because of the recesses and collar pipes and
- MPBXs could only be installed after some relaxation had occurred, except for the two MPBXs that were installed in the 12-Drift.

#### 4.3.2 Multiple-Point Borehole Extensometer Measurements

The data for the MPBX measurements were presented in Figures 2-1 through 2-4 in Report B. The data are replotted here for one time period to study the relaxed zone. Figures 4-2, 4-3, and 4-4 are plots of MPBX-related displacements. The plots are for J-Day 145 (1986), which was selected as a common time for illustrating the relative displacements of the anchors after the blasting at Station E. A review of Figures 2-1 through 2-4 in Report B shows that the relative displacements are reasonably uniform and that the selection of data from this one day should not lead to erroneous conclusions. The plots provide the anchor displacements relative to the bottom anchor so that the displacements are assumed to be zero at the bottom anchors for all but MPBXs C7 and E7, where the zero displacements are at the collar.

Figures 4-2, 4-3, and 4-4 are used for relaxed zone determinations and for numerical model/measurement comparisons in the rock mass. The model results are presented in Appendix A. The numerical model curves are discussed in Section 4.5. The relaxed zone determinations are presented first. The shapes of the numerical model plots and not the magnitudes are used in relaxed zone determinations. It is assumed in this document that some manifestation of inelastic rock response occurred in the relaxed zone when the measurements deviated significantly from the predicted shape.

Comparisons of measured results with predicted shapes in Figure 4-2 show that differences were not significant. In considering the overall comparisons, it would be difficult to attribute any relaxed zone effects to the roof behavior.

Figure 4-3 shows the results for the floor measurements and the model predictions at Stations C and E. There are two qualifications that should be reiterated before discussing this figure. The first is that the MPBXs were in different strata in the floor. At Station C, the MPBX was in the

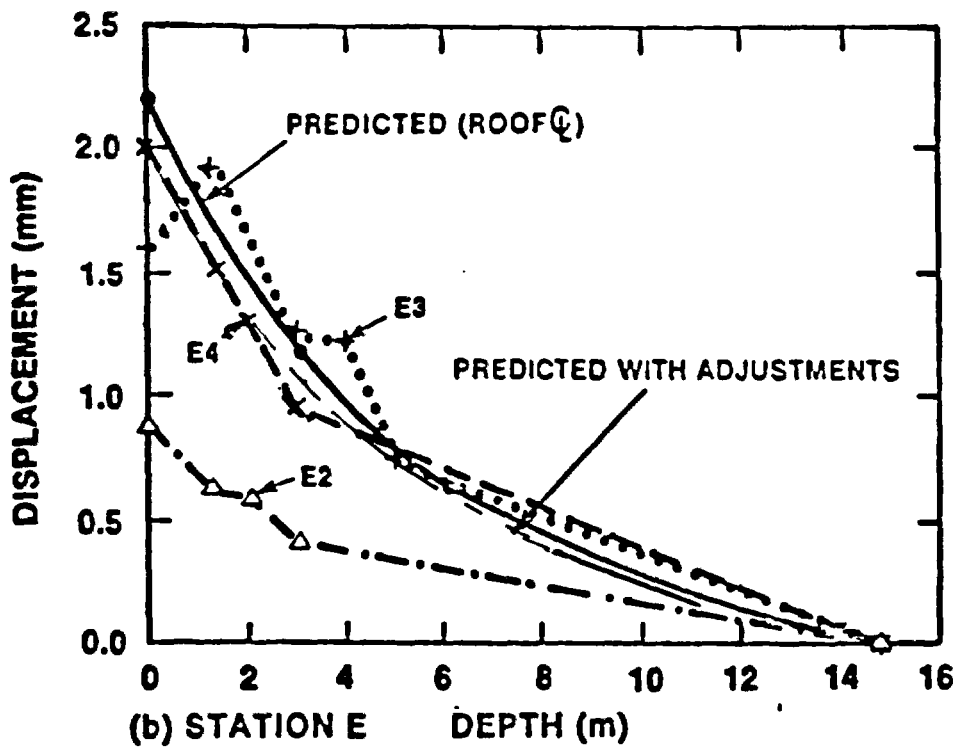
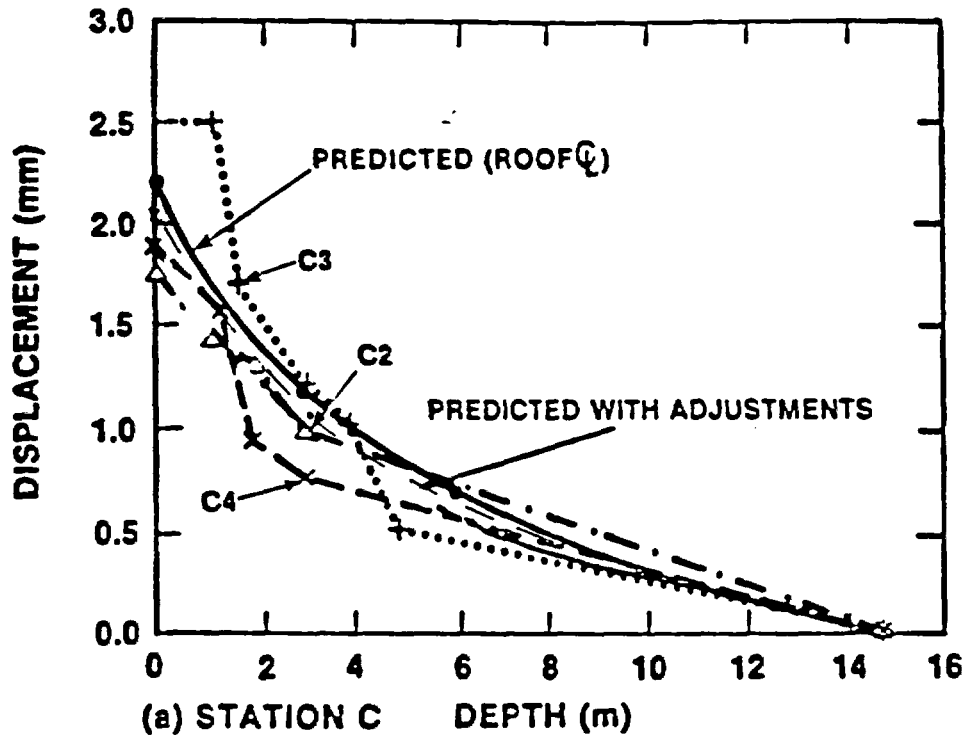


Figure 4-2. Comparisons of Roof Multiple-Point Borehole Extensometer Data and Model Results for J-Day 145 (1986)

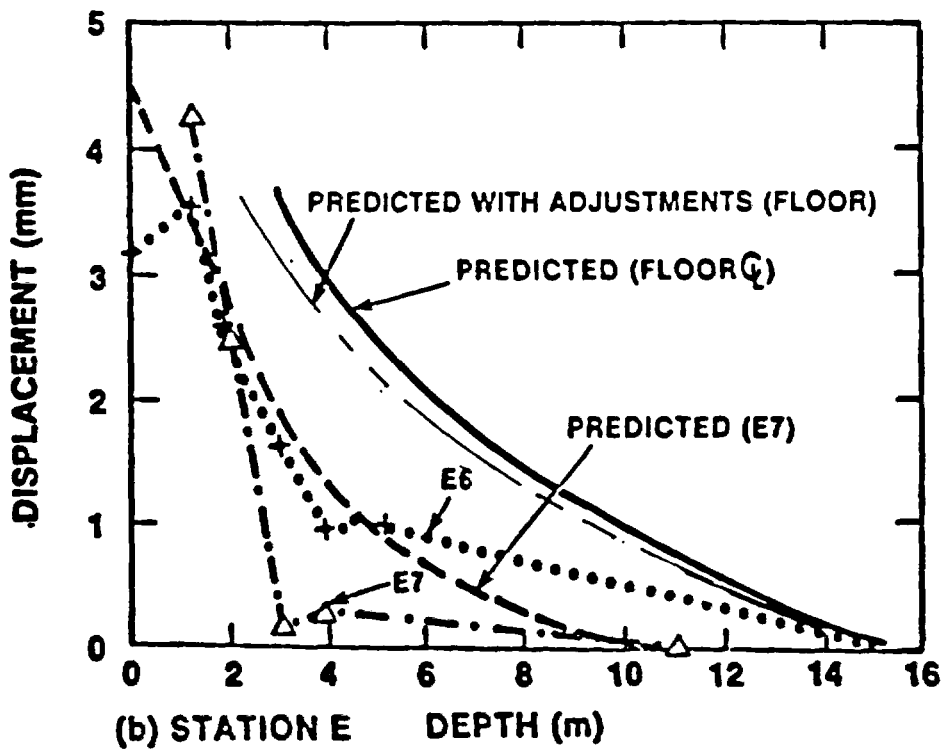
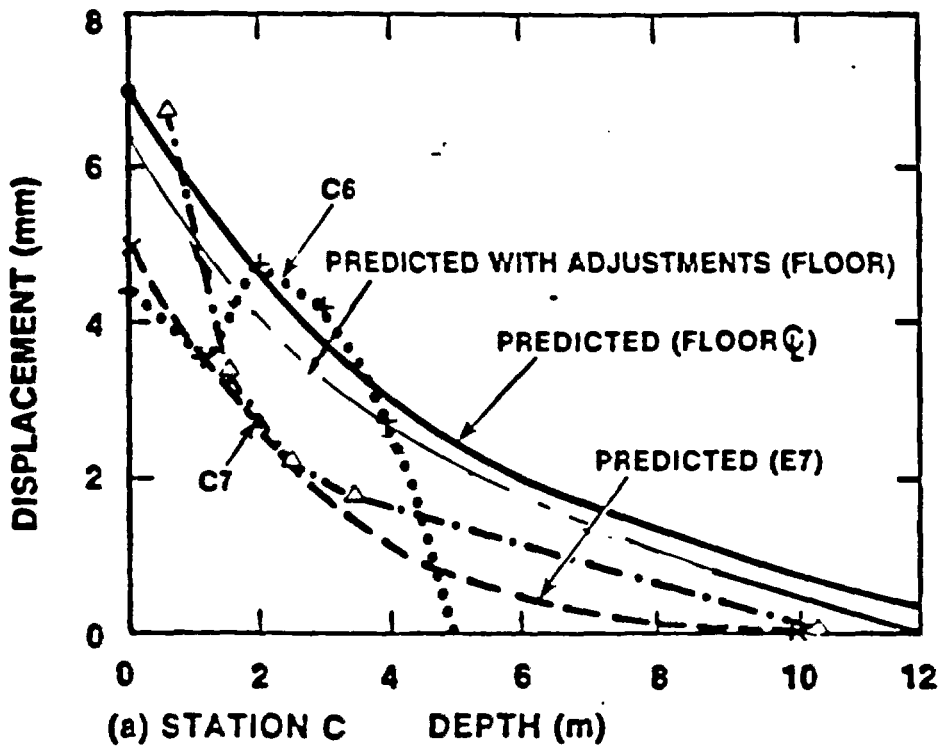


Figure 4-3. Comparisons of Floor Multiple-Point Borehole Extensometer Data and Computer Output for J-Day 145 (1986)

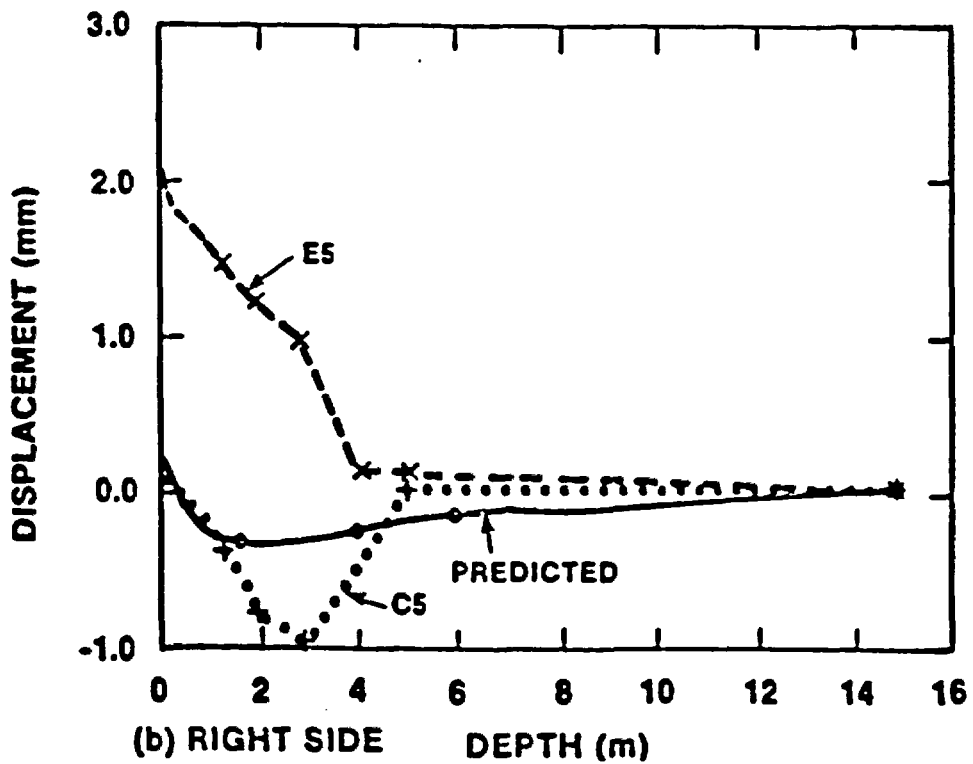
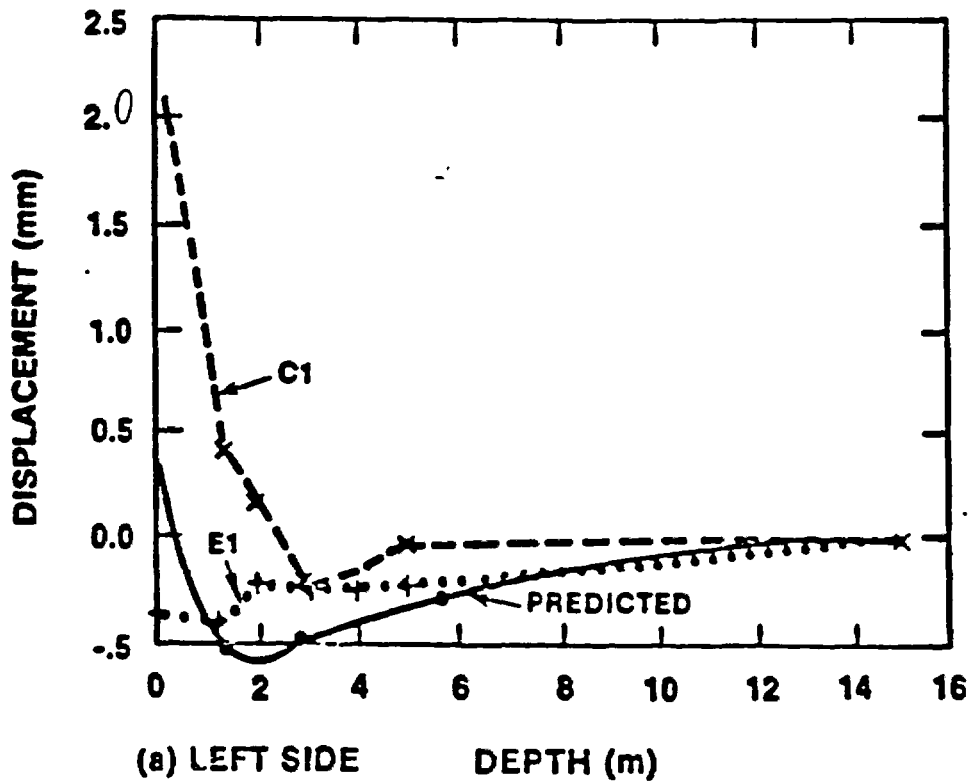


Figure 4-4. Comparisons of Horizontal Multiple-Point Borehole Extensometer Data and Computer Output for J-Day 145 (1986)

rubble zone, and it was at the top of the vitrophyre at Station E. Second, the bottom anchor for MPBX C6 was inoperative and the displacements were referenced to the next-to-last anchor, located at a depth of 5 m.

Figure 4-3a shows that the vertical anchor movements follow the model values within reason. The only distinct region of difference is between the MPBX C6 collar and the anchor at a depth within a 2-m distance. This measurement occurred in the rubble zone and would be difficult to characterize. Figure 4-3b shows that the measured values for MPBX E6 were generally regular, and it would be difficult to assess relaxed zone effects. These measured results were possibly influenced by the stiffer vitrophyre.

Figure 4-3 also shows the measurements from the inclined MPBXs, with origins in the 12-Drift. It is noted that the slope of the displacement gradient increased within the 1.5-m range for MPBX C7. There was a minor variation in the pattern for MPBX E7 in the 3- to 4-m range, and then the displacement gradient increased in a manner similar to MPBX C7. The variation in the 3- to 4-m range could have been some relaxed zone development in the stratified floor.

Figure 4-4 shows the comparisons of the horizontal MPBX relative anchor displacements and the corresponding model predictions. This figure shows the greatest measurement deviation from the predicted shapes.

Figure 4-4a shows a comparison of the south side displacements and the model predictions. Two things are evident. There is a significant deviation from the MPBX C1 measurements and the model at the 3-m anchor. On the other hand, displacements from MPBX E1 showed only minor variations within a distance of 2 m.

Figure 4-4b shows the results for the north side of the two stations. The figure shows that the horizontal displacements at Stations C and E

generally deviated from the predicted shapes. There was additional variation in the MPBX C5 displacement pattern at a depth of 3 m.

As a general observation regarding the horizontal displacements, the greatest deviations from the horizontal measurements and the model occurred with the MPBXs that were located nearest the fault intersection. This would be expected because the fault intersected the Demonstration Drift at an angle. This strongly suggests that the fault had an impact on the measurements and that some form of shear zone developed in the relatively unsupported sidewalls during the excavation.

There is also the possibility for wall slabbing. Figure 2-4 shows that the only wall support consisted of rock bolts near the intersection with the arched roof. This is in the zone of higher compressive stresses. Fairhurst and Cook (1966) pointed out that splitting parallel to the direction of the maximum compressive stress is the principal mode of macroscopic fracture in brittle rock. They reported that a highly stressed brittle rock is composed of incipient slabs produced by partial cleavage parallel to the face. Eventually, some of the incipient slabs can fail by buckling. The authors point out that short rock bolts or arches can be used to stabilize the buckling of the slab if the stress is so great that cleavage cannot be prevented. The increased displacement gradients noted with MPBXs C1, C5, and E5 near the surface would support the slabbing phenomenon. The evidence is that there was some loosening in the horizontal direction. The drift convergence rates in the horizontal direction were small. A review of the displacement histories does not suggest that the loosening caused any significant slabbing instabilities to develop.

#### 4.4 Summary of Relaxed Zone Evaluations

The relaxed zone has been defined as that zone around the perimeter of an excavation where there are rock property changes resulting from the blasting and rock removal. Previous studies indicate that blast damages can be defined in three zones whose total region of influence is normally contained within one-half the spacing of the perimeter holes in controlled

blasting but can be up to 1 m in discontinuous rock. No evidence was found to dispute this within the limitations of our measurements.

The authors were able to determine apparent effects of stress redistributions. Results from the HQ measurements in six boreholes at Stations B, D, and F showed that there was an apparent gravity-influenced zone in the fault that was closest to Station D. This demonstrates that the pre- and postmining measurement is feasible in detecting major changes in the rock as a result of stress alterations. The measurements showed that the rock was loosened up to a distance of 2.5 m. HQ measurements in other holes suggested that, if anything, there was a small amount of fracture tightening caused by the stress redistributions. The measurements were not taken where blast damage could be assessed, essentially within 1 m of the surface, and this is a limitation.

Results from roof-mounted MPBX measurements at Stations C and E showed that the roof was adequately held with the 3-m-long grouted rock bolts and that distinct loosening zones were not evident. The measurements nearest the surface were at a distance of over 1 m. No apparent blast damage effects beyond that distance were observed. Results from the unsupported floor-mounted MPBXs were apparently affected by stratigraphic variations, and relaxed zone effects were difficult to assess. Loosening up to a distance of 4 m was noted in the rock underlying the floor.

The horizontal measurements showed more significant loosening effects. Apparent shear zones were developed near the intersecting fault, as evidenced by the larger MPBX measurements nearest the fault where shear-induced displacements probably occurred. There is a potential for some wall slabbing in the sidewalls, but no instabilities were evident. In general, rock loosening up to 5 m from the opening was observed in the horizontal direction.

In summary, the three zones that were outlined by Cording et al. (1971) were evident in these measurements. First, there was a general

loosening in the roof zone in the vicinity of the fault, as measured with the HQs. The evidence was that the gravity zone appeared to have extended to a depth of 2.5 m in the roof. Second, the horizontal MPBX data suggested that there were larger displacements nearest locations where the fault intercepted the Demonstration Drift. There was evidence of rock loosening as deep as 5 m in the walls. Such behavior would suggest shear zone movement in the sidewalls. Slabbing-zone-type development in the walls was also postulated. The larger displacements within 2 m in the walls are attributed partially to slabbing zone developments. Finally, there was a loosening in the floor that was assumed to be some manifestation of the floor heave phenomenon.

#### 4.5 Rock Mass Measurement/Model Comparisons

The focus of the WTM Experiment was to measure the rock mass behavior. Comparisons of cross drift measurements with results from linear-elastic calculations have been made in Section 3.1.3.2. The purpose of this section is to make comparisons in the rock outside the drift surface. These more extensive comparisons allow numerical model limitations to be evaluated in more detail. In particular, these discussions address how some of the experiment practices and model limitations might be adjusted to achieve better measurement/model comparisons.

Figure 4-2 shows the comparisons for the roof displacements and related computations for Stations C and E. The figure shows computed displacements representing the MPBX measurement ranges. These are computed assuming the full drift excavation and are identified by the label Predicted (roof c1). The details and the limitations of the linear-elastic model are provided in Appendix A. One measurement limitation is that the MPBX data represent data approximately 0.5 m from the actual drift surface because of the presence of the recesses. Actual displacements might be slightly larger at the surface.

In the linear-elastic model, the measurements that were initialized near the edge of an unmined face were taken as 40% of the total elastic displacements (Section 3.1.3.2). In Chapter 3, the comparisons showed that the measured displacements were approximately 2.0 to 2.7 times the computed values. For the purposes of these discussions, it is assumed that the rock material properties in the model could be changed so that the differences in the measured and computed displacements could be resolved by increasing the predicted displacements by a factor of 2.35 (a convenient value between 2.0 and 2.7). If a ratio of 2.35 were combined with the factor of a 40% reduction mentioned earlier, the predicted displacements for comparison purposes should be 0.94 times those predicted in Figure 4-2. This is called the adjusted model output and is also shown in Figure 4-2.

Figure 4-2 shows that five of the six MPBX plots would be very close to the adjusted model output curves. This comparison suggests that something like the 2.35 factor could be used to adjust rock material properties defining the roof to give better measurement/model agreement. The comparison also suggests that additional factors must be considered if the measurement/linear-elastic-model comparison were to be improved (for all six MPBXs). The possibility exists that the deviant MPBX E2 was located in a portion of the rock that did not behave like the nearby rock or that it was installed differently than thought. From observations of the surface of the drift, it would have been almost impossible to map the fractures accurately enough to prepare a more elaborate three-dimensional model containing discrete fractures. This much variation between measured and predicted results may exist in making any measurement/model comparisons. If this is the case, it might be prudent to design experiments in the future to include enough redundancy to achieve statistical significance in critical measurements.

Figure 4-3 shows comparisons of the floor measurements and the linear-elastic model results for Stations C and E. The previously discussed ratio of 0.94 would apply only to the MPBX C6 and E6 data because they were initialized near a face. Figure 4-3a shows that three of the anchor

results for MPBX C6 compare favorably with the adjusted numerical model values. This comparison could be different if the data from the bottom anchor were available; thus, the comparison should not be weighed too heavily. Also, the drift was modeled for Station E, and the numerical results for the floor would be expected to be less accurate at the C Station. Figure 4-3b shows that the MPBX E6 displacements are uniformly lower than the adjusted numerical model outputs. Assuming negligible measurement errors, this comparison shows that again it would be difficult to improve the model by adding discrete fractures to a three-dimensional model. Perhaps the most judicious linear-elastic model improvement would be in changing the assumed rock material properties for the stratigraphic layers, but such action would have to be incorporated into a three-dimensional model.

A second set of comparisons is available in Figure 4-3. These comparisons involve the measurements and predicted displacements for the MPBXs with origins in the 12-Drift. In this case, the linear-elastic model displacements should not be reduced by the factor of 60% because the C7 and E7 MPBXs were installed before the mining of the Demonstration Drift. For comparisons to be compatible with the previous discussions, the predicted displacements should be increased by the assumed material property adjustment of 2.35. If this were done, both comparisons in Figure 4-3 would result in larger differences. There are several reasons why this could occur. First, the MPBX boreholes were percussion drilled and were not precisely aligned. Second, it is known that the floor levels were not constant as the distance from the floor to the top anchor varied from 0.6 m at Station C to 1.2 m at Station E. These locations are in high-displacement gradients, and location errors are important. Finally, BI activities may have influenced the floor more than the roof. From a modeling standpoint, this is the only comparison where the 12-Drift is factored in, and the possibility exists that the model describing the behavior between the 12-Drift and Demonstration Drift needs attention. It is apparent that just changing the material properties in the linear-elastic model will not bring all model predictions and measurements closer together, particularly where

floor behavior is concerned. Measurements appear to be influenced by non-linear rock behavior.

Figure 4-4 shows the comparisons between the horizontal MPBX outputs and the corresponding numerical model predictions. This figure shows the greatest deviations from the predictions. To be compatible with previous discussions, the predicted results should be multiplied by 0.94 to account for full-drift mining and assumed adjustments in material properties. The predicted displacements are small, and the adjusted model curves are not shown in Figure 4-4. Other factors should be mentioned. First, the MPBX anchors were located in a variable stratigraphy because of the dip of the units. Second, plots in Appendix A show that the horizontal displacements are extremely sensitive to positions along a horizontal line and that errors in anchor placement could impact results because of the displacement gradient. The MPBX heads were recessed 0.5 m.

Figure 4-4a shows the comparisons of the south side displacements and the model predictions. Two things are evident. First, there was a significant deviation from Borehole C1 measurements beginning at the 3-m anchor. This is perhaps a result of the rock loosening or rock slabbing in that region. The relatively small negative displacements at Station E in Figure 4-4a show the best comparisons with the model predictions. An inspection of the MPBX locations shows that there was more overbreak there, and the possibility exists that the rock was forming more of an arch, which was predicted with the model.

Figure 4-4b shows the results for the north side comparisons for the two stations. The figure shows that the horizontal displacements at Station E were significantly larger than predicted up to a depth of 4 m. Deep within the rock, the predicted displacements were small and opposite in polarity to those predicted. The measurement patterns suggest that there was general side wall convergence at Station E and that the range of significant deformation extended out to a distance of 4 m. Again, this could be related to the influence of the shear zone and possibly a slabbing

phenomenon. Comparisons of the predicted and measured values at Station C show that the C5 displacements generally followed the trends with greater displacements in the 1 to 4 m range. The authors believe that the measured displacements were influenced by the rock loosening in that region.

In review, six model limitations were discussed in reference to those comparisons (Appendix A). The major model modifications that were feasible were to (1) improve material property descriptions and (2) provide for discontinuities.

The measurement/linear-elastic model comparisons in the rock mass have shown that there are limitations to what can be done. In considering the first of the two factors mentioned in the previous paragraph, there appears to be measurement scatter that may not be corrected with improved material property descriptions or even model improvements. There is evidence that measurement/model comparisons should be made using a statistical approach. This observation suggests that experiments should be designed with this in mind.

The second of the two model limitations dealt with discontinuities. The comparisons and discussions in this section have considered only linear-elastic models. It is assumed that a three-dimensional model, possibly with discrete fracture definitions, would be an improvement. It is possible that a compliant-joint model (Thomas, 1982) could be applied to some advantage. The effects of joints in a linear-elastic model are approximated by using a reduced modulus of deformation. A restraint in the linear-elastic model used is that there are predicted capabilities for the rock to withstand tensile stresses. This may not be the case in a fractured rock mass. The compliant-joint model offers the advantage that the rock mass is treated as an elastic medium in which there is (1) allowance for nonlinear joint normal compliance and shear behavior and (2) provisions for restricting tensile stress buildups. The capabilities for defining a low shear stiffness and the absence of tensile stress buildups means that energies are transferred to a larger volume of rock and this may

be more realistic. It would be useful to apply a compliant-joint model to the conditions here to assess potential advantages or limitations.

#### 4.6 Rock Mass Hydraulic Properties

The HQ measurement concept was designed to assess changes in the rock mass without requiring precise definitions of many of the physical properties and relationships. The HQ application involved measurements of flow rate and pressure under pre- and postmining conditions. Measurements of these two quantities can be used for making rough estimates of the rock mass hydraulic properties; that is the intent of this section. The HQ measurements were the first measurements in welded tuff where flow rate and pressure relationships were measured in sequential intervals. Zimmerman and Vollendorf (1982) took similar types of measurements at selected fractures in the welded tuff, but there was no attempt to characterize large volumes of the rock mass. The information presented here represents the results from measuring hydraulic properties in six boreholes covering a total length of over 25 m.

##### 4.6.1 Aperture Changes

Aperture determinations appear to be a common reference quantity to determine mechanical changes in the rock mass. The HQ evaluations were not designed to calculate apertures, but upper bound values can be estimated. The calculated values represent an upper bound because the number of fractures ( $n$ ) in the reference Equation 3-1 in Report B is assumed to be unity. The equation is rewritten to emphasize the hydraulic aperture ( $e$ ) and is

$$e = \left( \frac{12 \cdot \mu \cdot \ln(l/r) \cdot 0.1 \cdot 10^7}{2 \cdot \pi \cdot H_0 \cdot \gamma_w \cdot n} \right)^{1/3} \quad (4-1)$$

Assuming a temperature of 20°C, the quantities other than Q and H<sub>0</sub> can be found to be

$$\mu = 1.002 \cdot 10^{-7} \text{ N} \cdot \text{s}/\text{cm}^2$$

$$l = 60.96 \text{ cm}$$

$$r = 3.81 \text{ cm}$$

$$n = 1$$

$1 \cdot 10^7$  = quantity converting units of  $\text{m}^3/\text{s} \cdot \text{kPa}$  to  $\text{cm}^5/\text{N} \cdot \text{s}$ .

Note: The quantity  $\gamma_w$  is not needed because it is incorporated into the HQ expressions through the units conversion.

Combining the quantities results in

$$e = (5.30 \cdot \text{HQ})^{1/3} \text{ (cm)} \quad (4-2)$$

All of the premining data that were used in the comparisons in Figure 4-1 were averaged, and the mean HQ for these 42 quantities was  $1.66 \times 10^{-7} \pm 2.68 \times 10^{-7} \text{ m}^3/\text{s} \cdot \text{kPa}$ . The individual quantities are listed in Table 4-1. A review of Figure 4-1 shows that there is a larger HQ at the beginning of Borehole B3 than is shown in Table 4-1. This data point is outside the sample population, and inclusion of it would cause the average to be shifted more than seems reasonable to arrive at a single value to represent the welded tuff. As shown in Table 4-1, the HQ quantities vary over three orders of magnitudes, and the standard deviation for the average shows this wide distribution.

Using Equation 4-2 and the average of the HQ quantities, the average hydraulic aperture for a single fracture in the sample intervals would be  $96 \mu\text{m}$ . Equation 4-2 has been applied to the individual HQs in Table 4-1. The average hydraulic aperture of those calculated from the HQs in the table is  $78 \pm 48 \mu\text{m}$ , and the range is from 36 to  $190 \mu\text{m}$ . Zimmerman and Finley (1987) reported the average single-fracture hydraulic aperture from their survey as  $90 \pm 59 \mu\text{m}$ . It could be argued that the average hydraulic aperture of  $78 \mu\text{m}$  should be used to describe the welded tuff, but if it

TABLE 4-1

SUMMARY OF PREMINING HYDRAULIC QUOTIENT  
MEASUREMENTS IN WELDED TUFF

<u>Borehole</u>	<u>Depth</u> <u>(m)</u>	<u>HQ</u> <u>(m<sup>3</sup>/s·kPa)</u>	<u>Borehole</u>	<u>Depth</u> <u>(m)</u>	<u>HQ</u> <u>(m<sup>3</sup>/s·kPa)</u>
B2	15.8	7.61 E-7	F2	15.8	1.97 E-8
	16.5	3.78 E-7		16.5	1.46 E-8
	17.1	4.13 E-8		17.1	1.85 E-8
	17.7	8.14 E-8		17.7	1.52 E-8
	18.3	5.77 E-7		18.3	1.59 E-8
	18.9	2.82 E-7		18.9	1.60 E-8
	19.5	4.22 E-8		19.5	1.91 E-8
B3	16.5	4.10 E-7	F3	16.5	3.48 E-8
	17.1	2.32 E-7		17.1	2.74 E-7
	17.7	2.07 E-8		17.7	3.30 E-7
	18.3	1.21 E-7		18.3	3.40 E-8
	18.9	1.30 E-6		18.9	1.72 E-8
	19.2	3.17 E-7		19.5	2.09 E-8
	19.8	2.45 E-7		20.1	3.90 E-8
	20.1	2.30 E-7		20.7	7.89 E-7
	20.7	2.36 E-8			
	21.3	1.14 E-7			
D2	16.5	1.16 E-8	<u>Distributions</u>		
	17.1	1.56 E-8	<u>HO</u>	<u>e</u>	<u>Total</u>
	17.7	1.34 E-8			<u>Number</u>
	18.3	1.25 E-8	> 10 <sup>-6</sup>	0.0174 cm	1
	18.9	1.30 E-8	> 10 <sup>-7</sup>	0.0081 cm	15
19.5	1.37 E-8	> 10 <sup>-8</sup>	0.0038 cm	41	
D3	16.5	1.07 E-8	> 10 <sup>-9</sup>	0.0017 cm	42
	17.1	9.10 E-9	1.66x10 <sup>-7</sup>	0.0096 cm	mean
	17.7	1.27 E-8			
	18.3	1.07 E-8			

were used, then flow rate predictions in Equation 4-1 would be distorted because of the averaging of nonlinear quantities. It seems that the value of  $96 \mu\text{m} \pm 59 \mu\text{m}$  is a reasonable representation of the upper limit hydraulic properties that were measured, and it is used in subsequent calculations. As an additional point of interest, the average hydraulic

aperture would be reduced to 76  $\mu\text{m}$  if it were assumed that there were two fractures in each measurement interval.

Table 4-1 also lists HQ and hydraulic aperture distributions. The distributions show that the measurements are skewed toward the smaller quantities.

It is interesting to evaluate the major changes in pre- and postmining rock behavior using apertures. Figure 4-1b shows that the HQ for both Boreholes D2 and D3 changed from approximately  $2 \times 10^{-8}$  to  $2 \times 10^{-6}$  as a result of the mining. It is assumed that this was a loosening of the rock in the fault zone. Using Equation 4-2, this would correspond to an equivalent single fracture hydraulic aperture increase of 173  $\mu\text{m}$ . This clearly shows that there was some relaxation as a result of the mining. This crude estimate of the aperture opening compares somewhat with the results of the G-Tunnel Heated Block Experiment. Zimmerman et al. (1986) showed that the hydraulic aperture in that experiment opened 65  $\mu\text{m}$  during the excavation of the block. A major difference in the two measurement conditions was that the roof of the Demonstration Drift was under the action of gravity, while the opening in the heated block resulted from relaxation of the horizontal stress field.

#### 4.6.2 Conversion of Hydraulic Quotient Measurements to Permeability Values

The premining data shown in Table 4-1 can be used to provide a general description of the fractured welded tuff. This information can be used by hydrologists in assessing the general characteristics of the welded tuff. The average of the premining HQ quantities for welded tuff for the six holes is  $1.66 \times 10^{-7} \text{ m}^3/\text{s}\cdot\text{kPa}$ . If all of the flow were assumed to occur in one fracture located in a measurement interval of 0.6 m, the average HQ quantity and corresponding saturated hydraulic aperture of 96  $\mu\text{m}$  could be converted to an equivalent upper-bound saturated hydraulic conductivity using the methods outlined in the Rock Testing Handbook (1980). The average value would be 0.75 cm/s. The value falls within the range

reported by Zimmerman and Vollendorf (1982) of 0.022 to 1.923 cm/s. At 20°C, the conversion factor from hydraulic conductivity to intrinsic permeability is  $1.02 \times 10^{-5}$  cm·s. Thus, the average value for the intrinsic permeability for an interval would be  $0.76 \times 10^{-5}$  cm<sup>2</sup>.

The welded tuff data can be compared with available data from granite rock masses. Montazer and Hustrulid (1983) discussed instrumentation and methods for conducting air permeability testing in crystalline rock masses. They performed injection measurements in three longitudinal holes, 30 m long, which were drilled parallel to an underground room. In addition, measurements were made in six sets of radial boreholes drilled within the room. There were seven boreholes, 4.6 to 9.1 m long, in each set. In the longitudinal holes, the injection interval was 2.13 m. They developed a method of testing where there was a 57% overlap to allow fracture location to within 30 and 50 cm in alternate interval spacings. The injection interval was reduced to 0.76 m for the radial boreholes, and the test interval spacing was 0.3 m. They reported air permeability values on the order of  $10^{-10}$  cm<sup>2</sup>.

Hodgkinson (1984) reported on the results of steady-state hydraulic injection tests into single fractures in a granite and developed a model to predict statistical fracture networks. The data collection consisted of injections into a rock mass at intervals of 1 m. A key parameter in the development of the model was the use of the ratio of flow rate/unit pressure, which is called the HQ in this document. Hodgkinson reported flow rate/unit pressure values varying from 0.24 to 1400 m<sup>3</sup>/s·MPa, which could be represented by an average hydraulic conductivity of  $1.4 \times 10^{-5}$  cm/s ( $1.4 \times 10^{-10}$  cm<sup>2</sup>).

Comparison with the granite shows that the welded tuff was approximately four orders of magnitude more permeable than the granite. As a final observation, Hodgkinson reported an average fracture frequency of 6.7 m, whereas Figure 4-1 shows that fracture zones appeared to occur in three to four 0.6-m intervals and that the maximum HQ quantities occurred in approximate 3-m intervals in three of the six holes. This means that

there appears to be swarms of fractures occurring at somewhat regular intervals. The swarm concept supports visual observations of the drift surface, but the periodicity is not clearly evident in visual observations. Thus, the HQ measurements suggest that, from a hydraulic standpoint, fractured welded tuff in G-Tunnel is significantly different from granite.

## 5.0 SUMMARY, CONCLUSIONS, AND RECOMMENDATIONS

The welded tuff mining experiment was established to document, analyze, and evaluate the premining, mining, and postmining behavior of a welded tuff during an excavation process. A drift, having dimensions of 29.6 m long, 6.1 m wide, and 4 m high, was mined in G-Tunnel. The drift was located in variable stratigraphy, with welded tuff on the roof and upper sides. A rubble zone intersected the bottom part of the drift at different elevations because of the presence of a normal fault (Report A\*). The fault, with a 2.5-m displacement, was located in the middle of the primary measurement system and affected the results to some degree. The location provided us with the opportunity to observe the effects of a structural discontinuity, and this proved to be useful in the final evaluations.

### 5.1 Summary for Evaluation of the Rock Performance During Excavation

#### 5.1.1 Evaluation of Drift Convergence Phenomena

Drift convergence magnitudes and rates were measured during the mining process to capture the behavior of the welded tuff so that information would be available for the design of similar-size drifts in the ES.

Drift convergence magnitude measurements were discussed in Chapter 3. The range of drift-closure measurements in the vertical direction was from 9 to 19 mm (Table 3-1), and a value of 13 mm was selected to be representative for the nonfaulted region. The measurements were compared with numerical model predictions; the ratio of TE measurements in nonfaulted rock to numerical predictions was 2.7 whereas the MPBX measurements showed a ratio of 2.0. Bieniawski and Maschek (1975) reported that similar ratios

---

\*Zimmerman et al., in prep. a.

under the magnitude of 3 indicated a loosening of the rock. Related zone evaluations in Chapter 4 indicated most loosening in the vicinity of the fault.

Vertical drift convergence rates ranged from 0.001 to 0.012 mm/day as measured with the TE. MPBX data showed the rates for the roof were 0.0003 to 0.0004 mm/day and for the floor were 0.0007 to 0.0017 mm/day. Analyses showed that floor heave that existed was most likely influenced by the variable stratigraphy and the tensile stress state. The floor heave would be expected to diminish with time based on G-Tunnel experiences.

A convergence rate of 0.001 mm/day would indicate stable conditions using a Bieniawski and Maschek (1975) criterion. If floor heave were discounted, the convergence values would be relatively small. Comparisons with available grouted rock bolt displacement capacities indicated that an estimated convergence rate of 0.001 mm/day would appear to be marginal for long-term roof support applications, but longer term measurements would be required to determine if 0.001 mm/day is realistic.

Drift convergence magnitudes in the horizontal direction ranged from 2 to 10 mm (Table 3-1) with TE measurements. The MPBX convergence measurements ranged from -0.5 to 2.4 mm. The horizontal convergence magnitudes appeared to be more directly influenced by the fault as the larger values were measured closest to the shear zone.

Horizontal convergence rates ranged from 0 to 0.005 mm/day when taken with TE measurements. The highest rates were in the shear zone near the fault. The rates decreased to less than 0.001 mm/day when computed from the MPBX measurements. These magnitudes and rates suggest that wall slabbing potentials are small.

### 5.1.2 Design of Predictive Capabilities

Empirical design methods were used to define the ground support system. These applications were discussed in Chapter 2. Applications

included the definition of the ground support system and the shape of the drift.

The actual rock mass classifications using the CSIR and NGI(Q) Systems were performed by Langkopf and Gnirk (1986). Based on these classifications, the PBQ&D-recommended ground support system called for grouted rock bolts. The primary ground support was resin-grouted rock bolts in a 1.2- x 1.5-m pattern with a woven wire mesh having a 5- x 5-cm grid. Different ground support systems were applied for demonstration purposes late in the mining phase. Gypsum and Portland cement grouts were used instead of resin in each of two rows. Swellex friction-type rock bolts were used in two rows to demonstrate another method of rock bolting. Finally, a fibercrete without wire mesh was added to approximately 6 m of drift. All appeared to perform adequately based on visual inspections.

A horseshoe shape with an arched roof was selected for the Demonstration Drift to accommodate the vertical to horizontal stress ratio of approximately 4 and to be generally consistent with the conceptual design for the repository. The radius of the arch at the roof of the drift was recommended by PBQ&D to be 0.6 times the drift width (W). A ratio of 0.72 W was eventually used to accommodate shape and geologic considerations.

### 5.1.3 Application of Control Blasting Technique

The control blasting technique applied was smooth blasting. The smooth blasting evaluations are discussed in Chapter 2. The goals in the smooth blasting were to minimize overbreak and develop good fragmentation, with full-face blasting. The overall perimeter control appeared to be adequate for the rock. The spacing of the holes appeared to be adequate. Some underbreak occurred and was corrected with secondary blasting. The largest overbreak was approximately 0.6 m, and this occurred in the faulted section. One item of note was that ANFO, a pneumatically loaded explosive, was difficult to apply in accurate amounts in the fractured rock.

The smooth blasting results were evaluated further in Chapter 4, where the excavation-caused relaxed zone was discussed. Displacement and HQ measurements were limited to beyond the first meter nearest the surface, but there was no evidence of blast damage in the regions where measurements were made. Results from borehole injection [hydraulic quotient (HQ)] measurements showed that there was an apparent excavation-induced loosening zone in the roof in the vicinity of the normal fault but that the roof remained relatively tight. Results from the roof-mounted MPBXs showed that distinct loosening zones were not evident. Loosening, to depths of 5 m in the horizontal direction, was observed using MPBX measurements.

#### 5.1.4 Conclusions on Performance of Rock During Excavation

- (1) The ground supports that were based in part on empirical rock mass classifications, NGI(Q) and CSIR, were adequate for the time period studied.
- (2) Convergence phenomena, magnitudes, and rates fall within the favorable ranges suggested by the Bieniawski and Maschek criteria, which were based on the behavior of other jointed rock types.
- (3) No ground support problems were encountered although a linear-elastic, numerical-model-predicted tensile zone exists in the roof of the drift.
- (4) The single, nonfaulted, representative value for measured displacements (13 mm) was 2.0 to 2.7 times the numerical model predicted displacements in the vertical direction. This value compared favorably with similar ratios established by Cording (1974).

- (5) The measured displacements were considerably larger than those predicted in the horizontal direction, perhaps because of shear zone effects and the absence of rock bolts.
- (6) The observed drift convergence phenomena consisted largely of initial convergence after blasting, and long-term convergences formed a small fraction of the total convergence magnitudes.
- (7) Support displacement capacities using grouted rock bolts 3 m long are adequate for short-term applications in welded tuff.
- (8) Smooth blasting techniques can be applied to fractured welded tuffs with moderate success.

#### 5.1.5 Recommendations for Future Rock Excavation Studies

- (1) A three-dimensional model, possibly with provisions for fractures, is needed to account for major structural features such as normal faults that were encountered in the Demonstration Drift.
- (2) Long-term convergences and support displacement capacities need to be studied for long-term repository applications.
- (3) Experiments need to be designed so that a statistically valid data base is developed to establish better measurement/model correlations. This implies using redundancy in measurements.
- (4) Considerations should be given to the use of tensioned rock bolts if support displacement capacities are to be studied.

## 6.0 REFERENCES

- Barton, N., F. Loset, R. Lien, and J. Lunde, "Application of Q-System in Design Decisions Concerning Dimensions and Appropriate Support for Underground Installations," V. 2, Subsurface Space, M. Bergman (ed.), 1974.
- Benson, R. P., D. K. Murphy, and D. R. McCreath, "Modulus Testing of Rock at the Churchill Falls Underground Powerhouse, Labrador," ASTM STP 477, Determination of the in Situ Modulus of Deformation of Rock, American Society for Testing and Materials, 1970.
- Bieniawski, Z. T., "Exploration for Rock Engineering," Proceedings of the Symposium on Exploration for Rock Engineering, Johannesburg, A. A. Balkema, Cape Town, South Africa, 1976.
- Bieniawski, Z. T., and R. K. Maschek, "Monitoring the Behavior of Rock Tunnels During Construction," The Civil Engineer in South Africa, V. 17, No. 9, 1975.
- Biffle, J. H., "JAC--A Two-Dimensional Finite Element Computer Program for the Non-Linear Quasistatic Response of Solids with the Conjugate Gradient Method," SAND81-0998, Sandia National Laboratories, Albuquerque, NM, April 1984.
- Brady, B. H. G., and E. T. Brown, Rock Mechanics for Underground Mining, George Allen & Unwin, London, 1985.
- Carroll, R. D., and J. H. Scott, "Uphole Seismic Measurements as an Indication of Stress Relief in Granitic Rock Tunnels," Paper 382-B, U.S. Geological Survey Professional Paper, 1966.
- Case, J. B., and P. C. Kelsall, "Modification of Rock Mass Permeability in the Zone Surrounding a Shaft in Fractured, Welded Tuff," SAND86-7001, IT Corporation Contractor Report to Sandia National Laboratories, Albuquerque, NM, March 1987.
- Cording, E. J., "Measurements of Displacements in Tunnels," Proc. 2nd Cong. AEG, Braz. Assoc. Engr. Geol., Sao Paulo, Brazil, 1974.
- Cording, E. J., A. J. Hendron, and D. V. Deere, "Rock Engineering for Underground Caverns," Underground Rock Chambers, ASCE, New York, NY, 1971.
- Dravo Engineers, Inc., "Effect of Variations in the Geologic Data Base on Mining at Yucca Mountain for NNWSI," SAND84-7125, Sandia National Laboratories, Albuquerque, NM, 1984.
- Fairhurst, C., and N. G. W. Cook, "The Phenomenon of Rock Splitting Parallel to the Direction of Maximum Compression in the Neighborhood of a Surface," Proc. 1st Cong. of the International Society of Rock Mechanics, Lisbon, Portugal, 1966.

Hodgkinson, D. P., "Analysis of Steady-State Hydraulic Tests in Fractured Rock," AERE-R 11287, DOE/RW/84.076, United Kingdom Atomic Energy Authority, Oxfordshire, UK, 1984.

Hoek, E., and E. T. Brown, Underground Excavations in Rock, The Institution of Mining and Metallurgy, London, England, 1980.

Johnson, R. L., and S. Bauer, "Preliminary Numerical Modeling for the G-Tunnel Welded Tuff Mining Evaluations," in preparation. SAND88-4001, Sandia National Laboratories, Albuquerque, NM.

Johnstone, J. K., R. R. Peters, and P. F. Gnirk, "Unit Evaluation at Yucca Mountain, Nevada Test Site: Summary Report and Recommendation," SAND83-0372, Sandia National Laboratories, Albuquerque, NM, June 1984.

Kelsall, P. D., J. B. Case, and C. R. Chabannes, "A Preliminary Evaluation of the Rock Mass Disturbance Resulting from Shaft, Tunnel, or Borehole Excavation," ONWI-411, D'Appolonia Contractor Report to Office of Nuclear Waste Isolation, Columbus, OH, 1982.

Langefors, U., and B. Kihlstrom, The Modern Technique of Rock Blasting, John Wiley and Sons, New York, NY, 1973.

Langkopf, B. S., and P. R. Gnirk, "Rock-Mass Classification of Candidate Repository Units at Yucca Mountain, Nye County, Nevada," SAND82-2034, Sandia National Laboratories, Albuquerque, NM, February 1986.

Miller, C. H., D. R. Cunningham, and M. J. Cunningham, "An Air-Injection Technique to Study Intensity of Fractures Around a Tunnel in Volcanic Rock," Association of Engineering Geologists, V. XI, No. 3, 1974.

Montazer, P. G., and W. A. Hustrulid, "An Investigation of Fracture Permeability Around an Underground Opening in Metamorphic Rocks," BMI/OCRD-4(5), Battelle Memorial Institute, Columbus, OH, 1983.

Montazer, P. G., G. Chitombo, R. King, and W. Ubbes, "Spatial Distribution of Permeability Around CSM/ONWI Room Edgar Mine, Idaho Springs, Colorado," Proceedings of the 23rd U.S. Symposium on Rock Mechanics, Berkeley, CA, 1982.

NRC (U.S. Nuclear Regulatory Commission), "Disposal of High-Level Radioactive Wastes in Geologic Repositories: Technical Criteria," Code of Federal Regulations, Energy, Title 10, Part 60, Washington, DC, 1981.

PBQ&D (Parsons Brinckerhoff Quade and Douglas), "G-Tunnel Welded Tuff Mining Excavations," PB/S 270-3836, PBQ&D, San Francisco, CA, report to Sandia National Laboratories, in preparation.

Pells, P. J. N., "The Behavior of Fully Bonded Rockbolts," Proc. 3rd International Congress on Rock Mechanics, ISRM, V. IIB, Denver, CO, 1974.

Rock Testing Handbook, RTH-381-80, U.S. Army Corps of Engineers, 1980.

Scott, J. H., F. T. Lee, R. D. Carroll, and C. S. Robinson, "The Relationship of Geophysical Measurements to Engineering and Construction Parameters in the Straight Creek Tunnel Pilot Bore, Colorado," International Journal of Rock Mechanics, Mining Sciences, and Geomechanics Abstracts, V. 5, 1968.

Simpson, R. E., J. E. Fraley, and D. J. Cox, "Inorganic Cement for Mine Roof-Bolt Grouting," RI 8494, U.S. Bureau of Mines, Washington, DC, 1980.

Siskind, D. E., and R. R. Fumanti, "Blast-Produced Fractures in Lithonia Granite," RI-7901, U.S. Bureau of Mines, Washington, DC, 1974.

Thomas, R. K., "A Continuum Description for Jointed Media," SAND81-2615, Sandia National Laboratories, Albuquerque, NM, April 1982.

Worsey, P. N., "In Situ Measurement of Blast Damage Underground by Seismic Refraction Surveys," Proc. 26th U.S. Symposium on Rock Mechanics, Rapid City, SD, 1985.

Zimmerman, R. M., and R. E. Finley, "Summary of Geomechanical Measurements Taken in and Around the G-Tunnel Underground Facility, NTS," SAND86-1015, Sandia National Laboratories, Albuquerque, NM, May 1987.

Zimmerman, R. M., and W. C. Vollendorf, "Geotechnical Field Measurements, G-Tunnel, Nevada Test Site," SAND81-1971, Sandia National Laboratories, Albuquerque, NM, May 1982.

Zimmerman, R. M., R. L. Schuch, D. S. Mason, M. L. Wilson, M. E. Hall, M. P. Board, R. P. Dellman, and M. L. Blanford, "Final Report: G-Tunnel Heated Block Experiment," SAND84-2620, Sandia National Laboratories, Albuquerque, NM, May 1986.

Zimmerman, R. M., R. A. Bellman, Jr., K. L. Mann, and D. P. Zerga, "G-Tunnel Welded Tuff Mining Experiment Preparations," SAND88-0475, Sandia National Laboratories, Albuquerque, NM, in preparation a.

Zimmerman, R. M., R. A. Bellman, Jr., K. L. Mann, D. P. Zerga, and M. Fowler, "G-Tunnel Welded Tuff Experiment Data Summary," SAND88-0474, Sandia National Laboratories, Albuquerque, NM, in preparation b.

Zimmerman, R. M., R. A. Bellman, Jr., and K. L. Mann, "G-Tunnel Welded Tuff Mining Experiment Instrumentation Evaluations," SAND88-1331, Sandia National Laboratories, Albuquerque, NM, in preparation c.

Zimmerman, R. M., K. L. Mann, R. A. Bellman, Jr., S. Luker, D. J. Dodds, and C. Sifre-Soto, "G-Tunnel Pressurized Slot Testing Evaluations," SAND87-2778, Sandia National Laboratories, Albuquerque, NM, in preparation.

APPENDIX A

TWO-DIMENSIONAL LINEAR ELASTIC MODEL PREDICTIONS

## A.1 DRIFT CONVERGENCE MODELING

The computations were performed with JAC, a finite element code (Biffle, 1984), using a two-dimensional linear elastic, plane strain model. Preliminary calculations were performed with this finite element code in designing the experiment to ensure that the instrumentation sensitivities were adequate. The models discussed here are the final linear-elastic representations of the test conditions (Johnson and Bauer, in prep.). For instance, in these calculations, the final dimensions of the Demonstration Drift were factored in.

### A.1.1 Two-Dimensional Model

The Demonstration Drift was modeled with a linear-elastic model to establish a reference base for other calculations. Figure A-1 shows the mesh that describes the model. The figure shows five different stratigraphic layers. The stratigraphic zones in the figure are a representation of the stratigraphy, and no attempt has been made in this two-dimensional model to factor in the fault. The layers were selected to represent the conditions near Station E so that the full stratigraphy could be easily represented with a mesh. The mesh was formulated to try to represent (1) the major features of the geometry of the two drifts, (2) the instrumentation and measurement locations, and (3) the variable stratigraphy.

The mechanical field-based properties for all but the rubble zone and in situ stresses were recommended by Zimmerman and Finley (1987) and are summarized in Table A-1. The values for the rubble zone were assumed. The values in Table A-1 represent quantities judged to be representative of the rock mass. The model was mathematically loaded with a vertical stress of 8 MPa and a horizontal normal stress of 2 MPa. The stresses were rounded values for the reference transformed stresses of 7.7 MPa (vertical) and 1.7 MPa (horizontal).

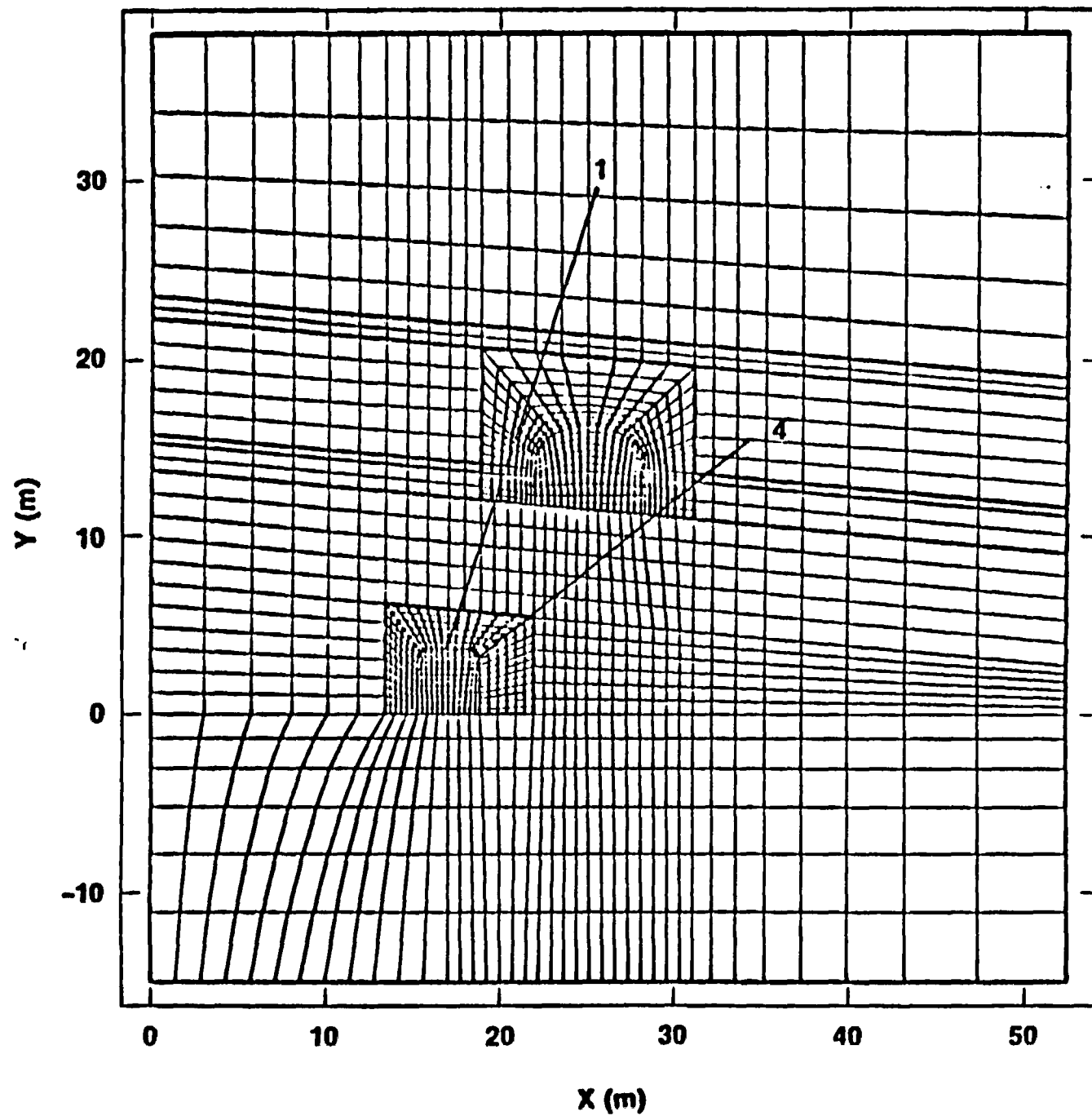


Figure A-1. Mesh for Welded Tuff Mining Evaluations--Linear Elastic Model

TABLE A-1

MATERIAL PROPERTIES FOR NUMERICAL MODEL\*

---

<u>Stratigraphic Zone Characteristics</u>	<u>Modulus of Deformation (GPa)</u>	<u>Poisson's Ratio</u>
I Nonwelded	8.6	0.21
II Nonwelded	7.1	0.22
III Moderately Welded	10.0	0.21
IV Densely Welded	16.0	0.29
V Rubble	5.9	0.21
VI Nonwelded	5.6	0.32

---

\*Zimmerman and Finley (1987).

---

The model was set up with assumptions of roller boundaries on the bottom and left sides and constant stress boundaries on the top and right. Global coordinates were referenced to the origin shown on Figure A-1, but the lower left-hand corner of the mesh was fixed in space for all calculations. Plots of model-predicted displacements are referenced to the global coordinates unless otherwise stated.

The boundary tractions were applied to establish the initial stress state in the mathematical mesh in the first of three steps. The second step was to mathematically remove the material within the 12-Drift boundary. The third step was to remove the material describing the Demonstration Drift. The elements within the two drifts were "removed" by reducing their stiffnesses to zero. In this way, we could assess the effects of the mining of the drifts in a realistic stress field.

A.1.2 Model Limitations

The two-dimensional linear-elastic model used here has inherent limitations as a result of specifications in the formulation of the material model. These limitations are summarized here.

- (1) Constant material properties within each stratigraphic zone-- There were no representations of anisotropy or nonlinear behavior.
- (2) Provisions for discontinuities--Joints, which may have nonlinear shear and normal compliance relationships, were not described.
- (3) In situ stress state--The stress state was assumed to be constant at boundaries, and there is no provision for changes with depth.
- (4) Time-dependent deformation--Time aspects such as creep and increased temperature were not considered.
- (5) Mesh representation--The mesh represents a finite volume of rock, and boundary conditions were assumed.
- (6) Ground support interactions--The model had no provisions for possible structural interactions of the ground support system.

### A.1.3 Model Results

Figure A-2 shows a plot of the calculated vertical displacements along the centerline of the Demonstration Drift. The calculations are for the third step of loading, i.e., after both the stresses were applied and the drifts were excavated. The plot is referenced to the roller boundary on the bottom. The plot shows that the floor is predicted to lift up 7.4 mm and that the roof is predicted to move 4.7 mm down relative to the bottom. Thus, there is a net predicted convergence of 12.1 mm across the drift. The figure also shows that there is a predicted net negative displacement of more than 2 mm at the top of the mesh, which is consistent with the stress boundary condition there. This residual displacement indicates that the excavation influences an even greater volume of rock than was defined with the mesh. The plot also shows that the mesh size is large enough so that meaningful displacements around the drifts are represented.

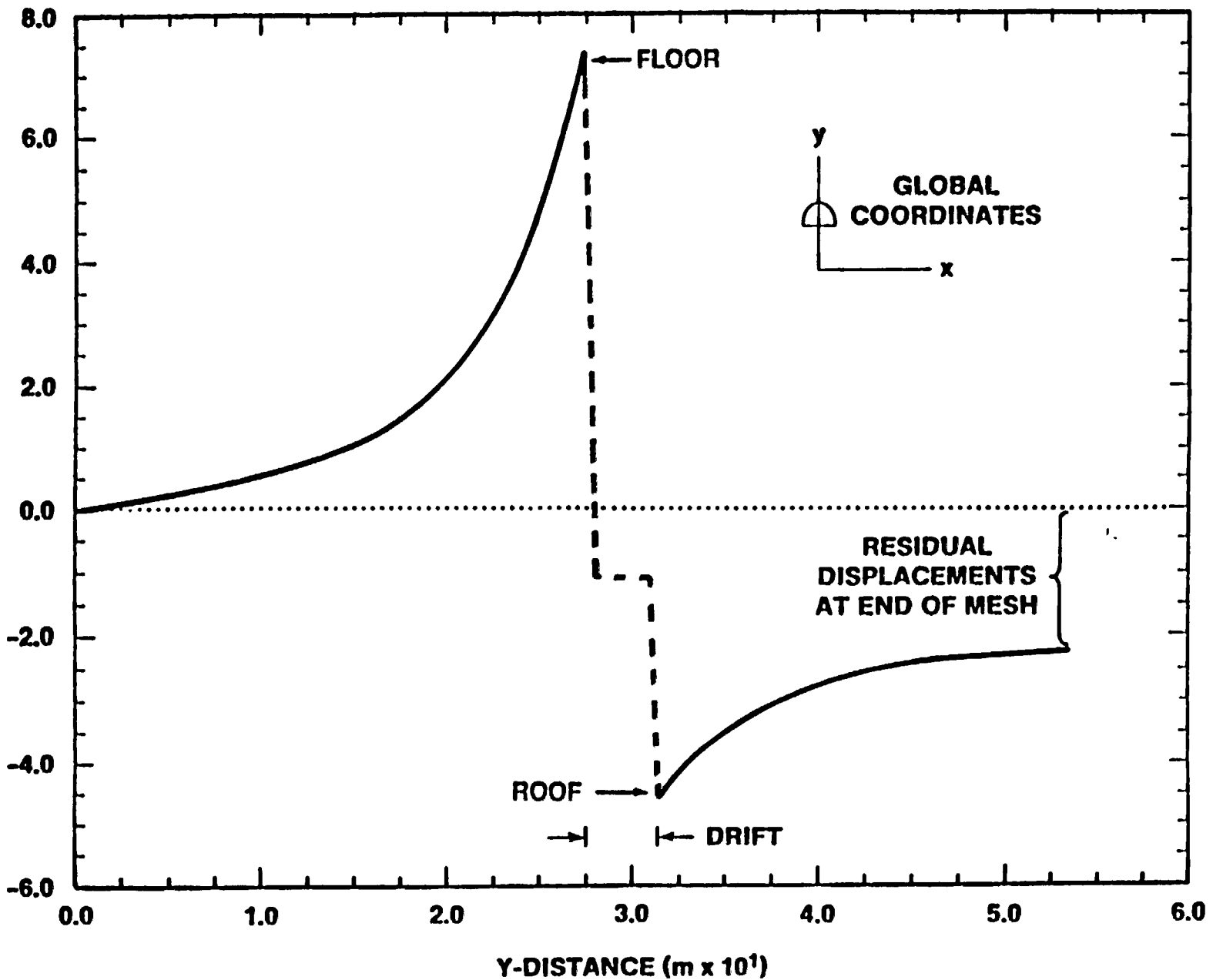


Figure A-2. Vertical Displacement Profile Along Centerline of Demonstration Drift

Figure A-3 shows two plots defining the displacements of the vertical MPBXs. The plots were made assuming zero displacement at a distance from the surface of 15 m, which would represent a bottom anchor relative MPBX measurement. The sign convention for the plots in Figure A-3 is that extension is positive. Figure A-3a shows that the predicted vertical relative displacement between the roof collar and the bottom anchor is 2.2 mm. Figure A-3b shows that the similar relative displacement between the floor anchor and the corresponding bottom anchor is 6.5 mm. Thus, the total predicted convergence for the region between the outlying anchors would be 8.7 mm, which is somewhat less than the 12.1 mm that was calculated for the entire mesh. This difference points out a limitation of the length of measurement region in selecting bottom anchor locations for MPBX measurements.

Figure A-4 shows a plot of the predicted horizontal displacements at midheight of the Demonstration Drift using global coordinates. The displacements are predicted for midheight to represent the MPBX locations. The calculations are for the third step of loading. The plots show that there were significant displacement gradients in the rock surrounding the surfaces of the drifts, yet the net convergences at the surfaces were zero. The general trend was for outward displacements (divergence) in the regions of the side walls immediately outside the surfaces. This divergence is judged to be a manifestation of the interaction of the arched roof and the side walls. The points of greatest divergence, having magnitudes of approximately 0.6 mm on the left and 1.0 mm on the right side, would be the effective thrust lines for the arch forming the roof. The thrust line concept is discussed in a later paragraph where stresses are emphasized. Once the maximum divergent displacements are reached, the following convergence trends are similar to those shown in Figure A-2. Figure A-4 also shows the residual displacement on the right side of the plot, which is related to the stress boundary condition.

Figure A-5 shows two plots that indicate the predicted MPBX displacements for the horizontal orientations. The displacements were referenced to the bottom anchors where extension into the drift is positive. There

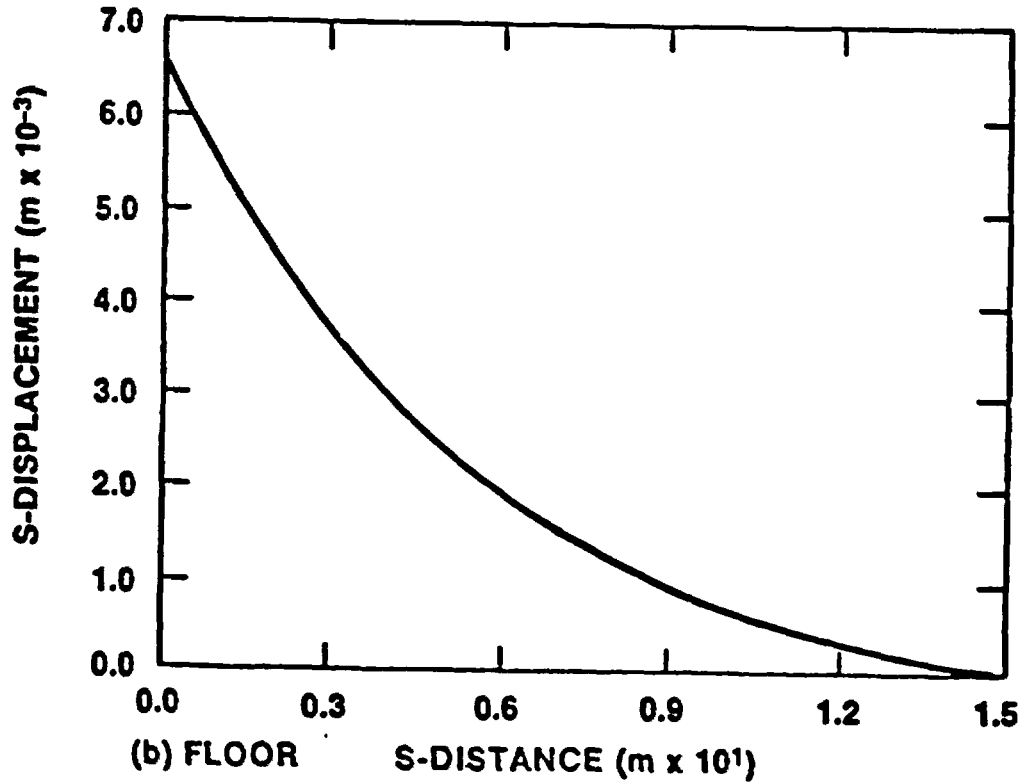
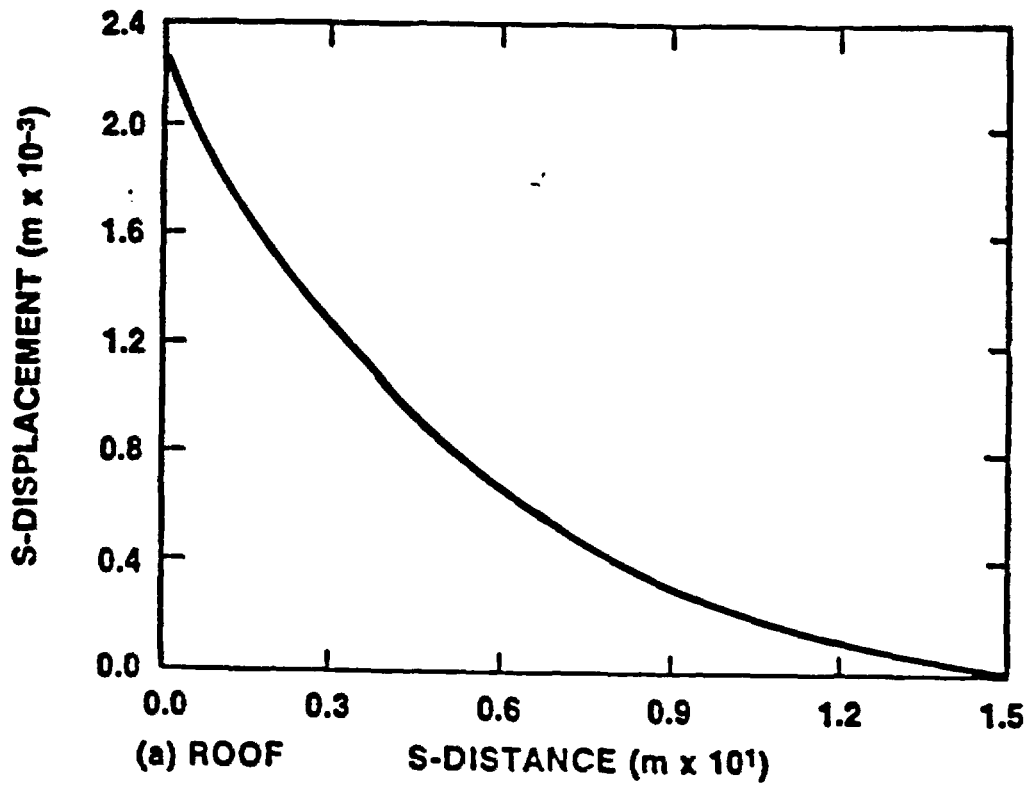


Figure A-3. Bottom Anchor Relative Predicted Multiple-Point Borehole Extensometer Displacement Profiles in Vertical Direction

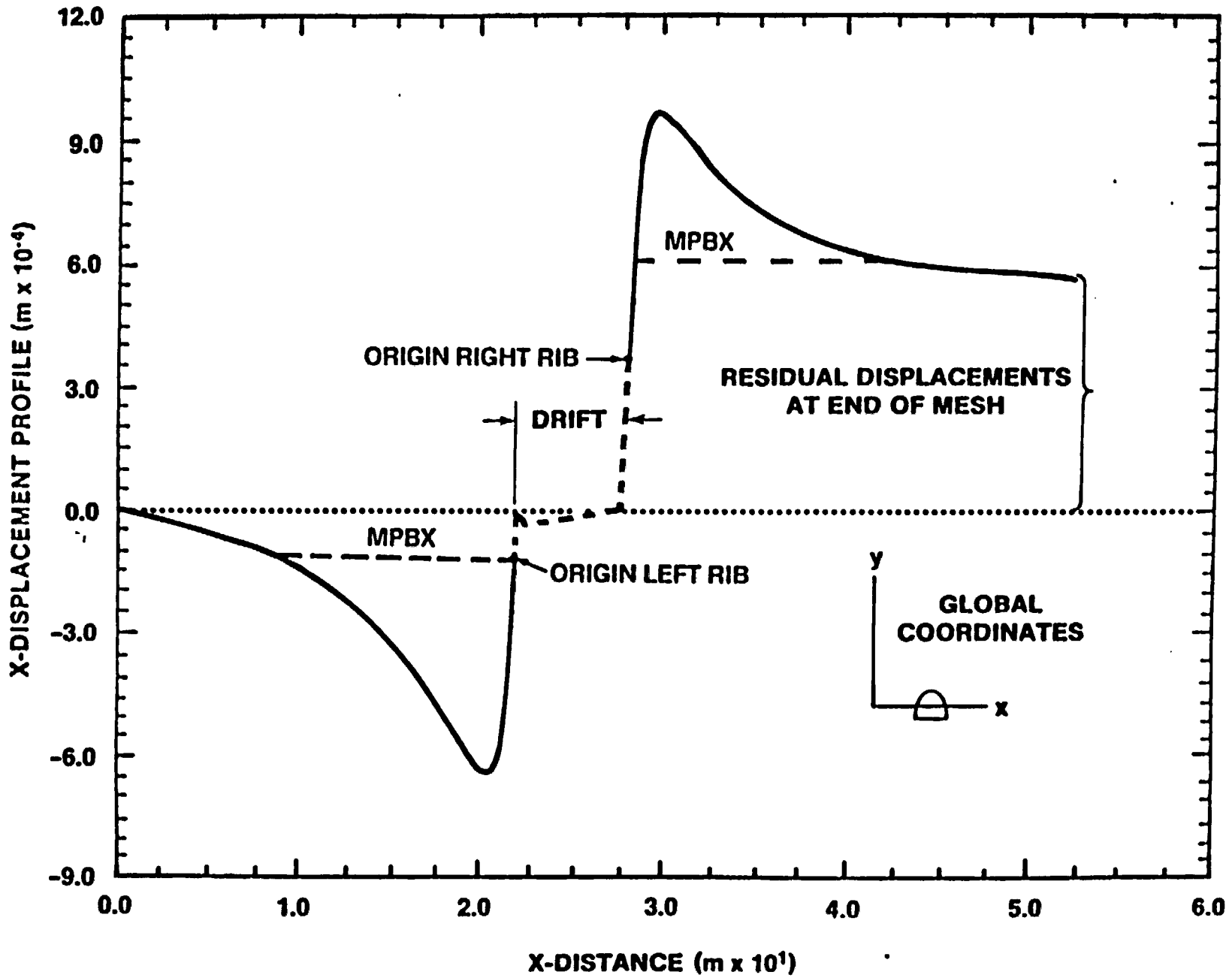


Figure A-4. Horizontal Displacement Profile at Mid-Height of Demonstration Drift

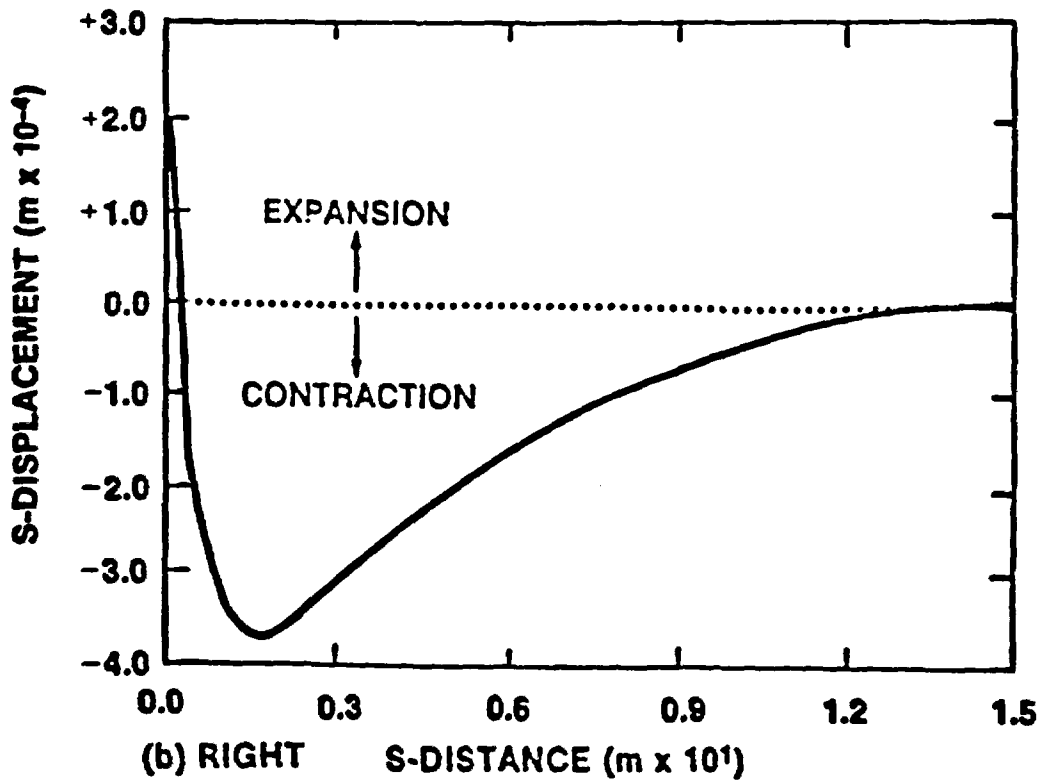
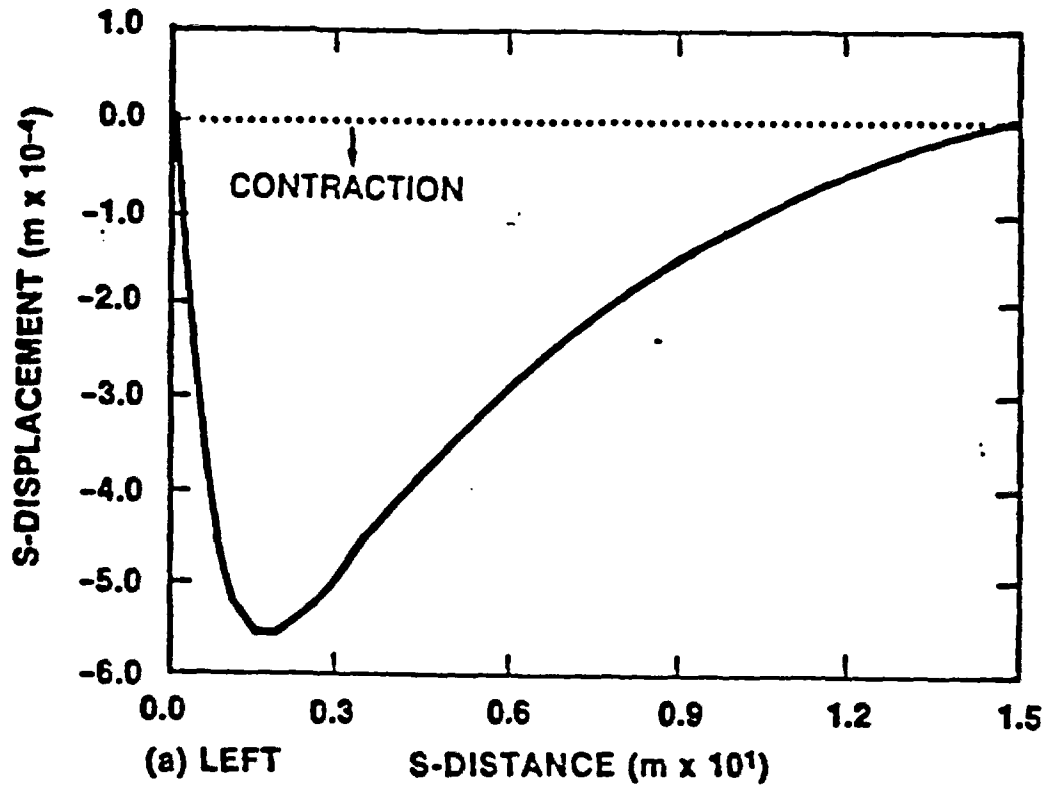


Figure A-5. Bottom Anchor Relative Predicted Multiple-Point Borehole Extensometer Displacement Profiles in Horizontal Direction

is a net convergence from the bottom anchors into the drift of 0.1 mm on the south side and 0.3 mm on the north side with these representations.

The predictive displacement trends are enhanced by an understanding of the stress distributions. Figure A-6 shows representations of the predicted vertical and horizontal stresses acting on the Demonstration Drift for loading step 3. Figure A-6a shows the vertical stress distributions. The figure shows a region near the sidewalls that has relatively high compressive stresses. This is the region that forms a hypothetical arch around the opening. The maximum vertical stress is predicted as 23.8 MPa near the spring line for the arched roof. Figure A-6 shows the predicted horizontal stresses.

Two items of special interest are evident in Figure A-6. First, the model predicts horizontal tensile stresses in the roof and floor for depths up to 1 m (Figure A-6a). The drift shape was designed without these model results, but analyses did call for a smaller radius for the arch (Report A\*). A larger radius was used to accommodate other considerations. This predictive tensile stress of 2 MPa is less than the tensile strength of the intact rock (Zimmerman and Finley, 1987). The tensile stress situation was possibly mitigated by the presence of the ground support system. Second, the maximum horizontal stress of 5.2 MPa in Figure A-6 is also near the spring line for the arched roof. Thus, the highest compressive vertical and horizontal stresses are predicted near the spring line for the arch.

---

\*Zimmerman et al. in prep. a.

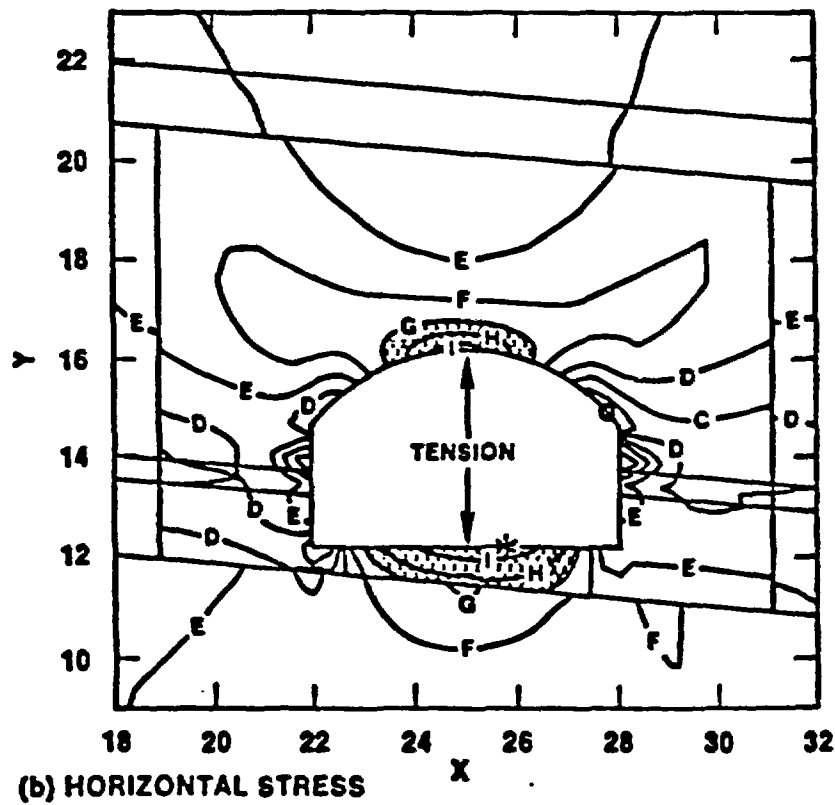
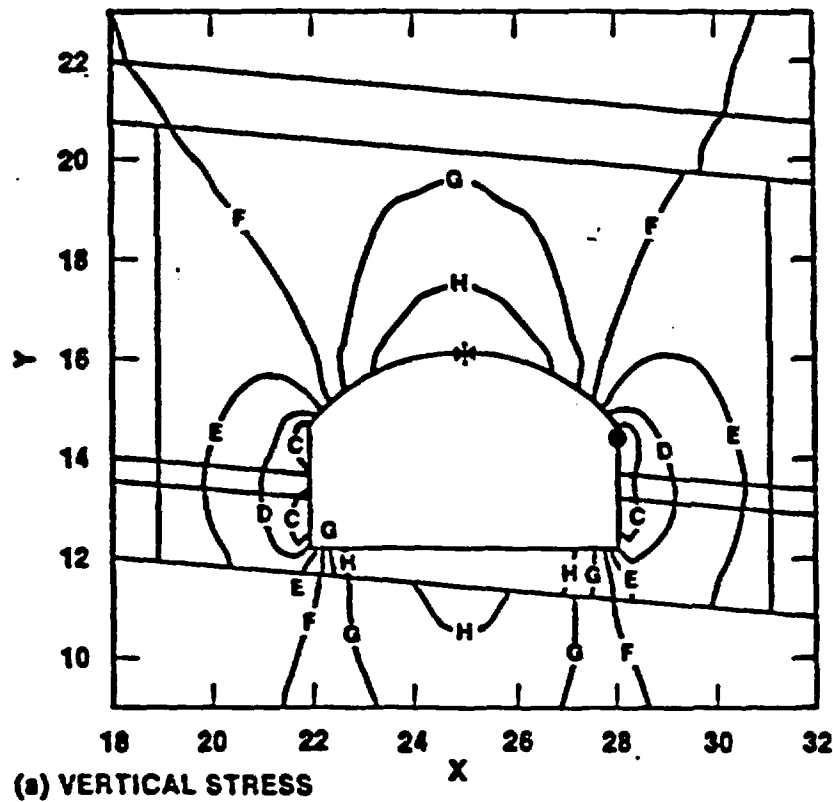


Figure A-6. Predicted Stress Distributions Around Demonstration Drift

APPENDIX B

Information from the Reference Information Base Used  
in this Report

This report contains no information from the Reference Information Base.

Candidate Information  
for the  
Reference Information Base

This report contains no candidate information for the Reference Information Base.

Candidate Information  
for the  
Site & Engineering Properties Data Base

This report contains no candidate information for the Site and Engineering Properties Data Base.

DISTRIBUTION LIST

Samuel Rousso, Acting Director (RW-1)  
Office of Civilian Radioactive  
Waste Management  
U.S. Department of Energy  
Forrestal Bldg.  
Washington, D.C. 20585

Ralph Stein (RW-30)  
Office of Civilian Radioactive  
Waste Management  
U.S. Department of Energy  
Forrestal Bldg.  
Washington, D.C. 20585

M. W. Frei (RW-22)  
Office of Civilian Radioactive  
Waste Management  
U.S. Department of Energy  
Forrestal Bldg.  
Washington, D.C. 20585

B. G. Gale (RW-23)  
Office of Civilian Radioactive  
Waste Management  
U.S. Department of Energy  
Forrestal Bldg.  
Washington, D.C. 20585

Samuel Rousso (RW-10)  
Office of Civilian Radioactive  
Waste Management  
U.S. Department of Energy  
Forrestal Bldg.  
Washington, D.C. 20585

J. D. Saltzman (RW-20)  
Office of Civilian Radioactive  
Waste Management  
U.S. Department of Energy  
Forrestal Bldg.  
Washington, D.C. 20585

S. J. Brocoun (RW-221)  
Office of Civilian Radioactive  
Waste Management  
U.S. Department of Energy  
Forrestal Building  
Washington, D.C. 20585

V. J. Cassella (RW-123)  
Office of Civilian Radioactive  
Waste Management  
U.S. Department of Energy  
Forrestal Bldg.  
Washington, D.C. 20585

S. H. Kale (RW-20)  
Office of Civilian Radioactive  
Waste Management  
U.S. Department of Energy  
Forrestal Bldg.  
Washington, D.C. 20585

T. H. Isaacs (RW-40)  
Office of Civilian Radioactive  
Waste Management  
U.S. Department of Energy  
Forrestal Bldg.  
Washington, D.C. 20585

D. H. Alexander (RW-332)  
Office of Civilian Radioactive  
Waste Management  
U.S. Department of Energy  
Forrestal Bldg.  
Washington, D.C. 20585

C. Bresee (RW-10)  
Office of Civilian Radioactive  
Waste Management  
U.S. Department of Energy  
Forrestal Bldg.  
Washington, D.C. 20585

Gerald Parker (RW-333)  
Office of Civilian Radioactive  
Waste Management  
U.S. Department of Energy  
Forrestal Bldg.  
Washington, D.C. 20585

Chief, Repository Projects Branch  
Division of Waste Management  
U.S. Nuclear Regulatory Commission  
Washington, D.C. 20555

NTS Section Leader  
Repository Project Branch  
Division of Waste Management  
U.S. Nuclear Regulatory Commission  
Washington, D.C. 20555

Document Control Center  
Division of Waste Management  
U.S. Nuclear Regulatory Commission  
Washington, D.C. 20555

Carl P. Gertz, Project Manager (5)  
Yucca Mountain Project Office  
Nevada Operations Office  
U.S. Department of Energy  
Mail Stop 523  
P.O. Box 98518  
Las Vegas, NV 89193-8518

J. L. Fogg (12)  
Technical Information office  
Nevada Operations Office  
U. S. Department of Energy  
P.O. Box 98518  
Las Vegas, NV 89193-8518

C. L. West, Director  
Office of External Affairs  
U.S. Department of Energy  
Nevada Operations Office  
P.O. Box 98518  
Las Vegas, NV 89193-8518

W. M. Hewitt, Program Manager  
Roy F. Weston, Inc.  
955 L'Enfant Plaza, Southwest  
Suite 800  
Washington, D.C. 20024

Technical Information Center  
Roy F. Weston, Inc.  
955 L'Enfant Plaza, Southwest  
Suite 800  
Washington, D.C. 20024

L. D. Ramspott (3)  
Technical Project Officer for YMP  
Lawrence Livermore National  
Laboratory  
Mail Stop L-204  
P.O. Box 808  
Livermore, CA 94550

M. E. Spaeth  
Technical Project Officer for YMP  
Science Applications International  
Corp.  
101 Convention Center Dr.  
Suite 407  
Las Vegas, NV 89109

H. N. Kalia  
Exploratory Shaft Test Manager  
Los Alamos National Laboratory  
Mail Stop 527  
101 Convention Center Dr.  
Suite P230  
Las Vegas, NV 89109

D. T. Oakley (4)  
Technical Project Officer for YMP  
Los Alamos National Laboratory  
N-5, Mail Stop J521  
P.O. Box 1663  
Los Alamos, NM 87545

L. R. Hayes (6)  
Technical Project Officer for YMP  
U.S. Geological Survey  
P.O. Box 25046  
421 Federal Center  
Denver, CO 80225

K. W. Causseaux  
NHP Reports Chief  
U.S. Geological Survey  
P.O. Box 25046  
421 Federal Center  
Denver, CO 80225

R. V. Watkins, Chief  
Project Planning and Management  
U.S. Geological Survey  
P.O. Box 25046  
421 Federal Center  
Denver, CO 80225

Center for Nuclear Waste  
Regulatory Analyses  
6220 Culebra Road  
Drawer 28510  
San Antonio, TX 78284

R. L. Bullock  
Technical Project Officer for YMP  
Fenix & Scisson, Inc.  
Mail Stop 403  
101 Convention Center Dr.  
Suite 320  
Las Vegas, NV 89109-3265

James C. Calovini  
Technical Project Officer for YMP  
Holmes & Narver, Inc.  
101 Convention Center Dr.  
Suite 860  
Las Vegas, NV 89109

Dr. David W. Harris  
YMP Technical Project Officer  
Bureau of Reclamation  
P.O. Box 25007 Bldg. 67  
Denver Federal Center  
Denver, CO 80225-0007

M. D. Voegelé  
Science Applications International  
Corp.  
101 Convention Center Dr.  
Suite 407  
Las Vegas, NV 89109

J. A. Cross, Manager  
Las Vegas Branch  
Fenix & Scisson, Inc.  
P.O. Box 93265  
Mail Stop 514  
Las Vegas, NV 89193-3265

P. T. Prestholt  
NRC Site Representative  
1050 East Flamingo Road  
Suite 319  
Las Vegas, NV 89119

A. E. Gurrola, General Manager  
Energy Support Division  
Holmes & Narver, Inc.  
P.O. Box 93838  
Mail Stop 580  
Las Vegas, NV 89193-3838

A. M. Sastry  
Technical Project Officer for YMP  
MAC Technical Services  
Valley Bank Center  
101 Convention Center Drive  
Suite P-113  
Las Vegas, NV 89109

B. L. Fraser, General Manager  
Reynolds Electrical & Engineering Co.  
P.O. Box 98521  
Mail Stop 555  
Las Vegas, NV 89193-8521

P. K. Fitzsimmons, Director  
Health Physics & Environmental  
Division  
Nevada Operations Office  
U.S. Department of Energy  
P.O. Box 98518  
Las Vegas, NV 89193-8518

Robert F. Pritchett  
Technical Project Officer for YMP  
Reynolds Electrical & Engineering Co.  
Mail Stop 615  
P.O. Box 98521  
Las Vegas, NV 89193-8521

Elaine Ezra  
YMP GIS Project Manager  
EG&G Energy Measurements, Inc.  
P.O. Box 1912  
Mail Stop H-02  
Las Vegas, NV 89125

SAIC-T&MSS Library (2)  
Science Applications International  
Corp.  
101 Convention Center Dr.  
Suite 407  
Las Vegas, NV 89109

Dr. Martin Mifflin  
Desert Research Institute  
Water Resources Center  
2505 Chandler Avenue  
Suite 1  
Las Vegas, NV 89120

E. P. Binnall  
Field Systems Group Leader  
Building 50B/4235  
Lawrence Berkeley Laboratory  
Berkeley, CA 94720

J. F. Divine  
Assistant Director for  
Engineering Geology  
U.S. Geological Survey  
106 National Center  
12201 Sunrise Valley Dr.  
Reston, VA 22092

V. M. Glanzman  
U.S. Geological Survey  
P.O. Box 25046  
913 Federal Center  
Denver, CO 80225

C. H. Johnson  
Technical Program Manager  
Nuclear Waste Project Office  
State of Nevada  
Evergreen Center, Suite 252  
1802 North Carson Street  
Carson City, NV 89710

T. Hay, Executive Assistant  
Office of the Governor  
State of Nevada  
Capitol Complex  
Carson City, NV 89710

R. R. Loux, Jr., (3)  
Executive Director  
Nuclear Waste Project Office  
State of Nevada  
Evergreen Center, Suite 252  
1802 North Carson Street  
Carson City, NV 89710

John Fordham  
Desert Research Institute  
Water Resources Center  
P.O. Box 60220  
Reno, NV 89506

Prof. S. W. Dickson  
Department of Geological Sciences  
Mackay School of Mines  
University of Nevada  
Reno, NV 89557

J. R. Rollo  
Deputy Assistant Director for  
Engineering Geology  
U.S. Geological Survey  
106 National Center  
12201 Sunrise Valley Dr.  
Reston, VA 22092

Eric Anderson  
Mountain West Research-Southwest  
Inc.  
Phoenix Gateway Center  
432 North 44 Street  
Suite 400  
Phoenix, AZ 85008-6572

Judy Foremaster (5)  
City of Caliente  
P.O. Box 158  
Caliente, NV 89008

A. T. Tamura  
Science and Technology Division  
Office of Scientific and Technical  
Information  
U.S. Department of Energy  
P.O. Box 62  
Oak Ridge, TN 37831

L. Jardine  
Project Manager  
Bechtel National Inc.  
P.O. Box 3965  
San Francisco, CA 94119

R. Harig  
Parsons Brinckerhoff Quade &  
Douglas  
1625 Van Ness Ave.  
San Francisco, CA 94109-3679

Dr. Roger Kasperson  
CENTED  
Clark University  
950 Main Street  
Worcester, MA 01610

Robert E. Cummings  
Engineers International, Inc.  
P.O. Box 43817  
Tucson, AZ 85733-3817

Dr. Jaak Daemen  
Department of Mining and  
Geotechnical Engineering  
University of Arizona  
Tucson, AZ 85721

Department of Comprehensive Planning  
Clark County  
225 Bridger Avenue, 7th Floor  
Las Vegas, NV 89155

Economic Development Department  
City of Las Vegas  
400 East Stewart Avenue  
Las Vegas, NV 89109

Planning Department  
Nye County  
P.O. Box 153  
Tonopah, NV 89049

Director of Community Planning  
City of Boulder City  
P.O. Box 367  
Boulder City, NV 89005

Commission of the European  
Communities  
200 Rue de la Loi  
B-1049 Brussels  
Belgium

Lincoln County Commission  
Lincoln County  
P.O. Box 90  
Pioche, NV 89043

Community Planning & Development  
City of North Las Vegas  
P.O. Box 4086  
North Las Vegas, NV 89030

City Manager  
City of Henderson  
Henderson, NV 89015

ONWI Library  
Battelle Columbus Laboratory  
Office of Nuclear Waste Isolation  
505 King Avenue  
Columbus, OH 43201

Librarian  
Los Alamos Technical  
Associates, Inc.  
P.O. Box 410  
Los Alamos, NM 87544

6300 R. W. Lynch  
6300-1 T. O. Hunter  
6310 J. E. Stiegler, Actg.  
6310 NNWSICF  
6311 A. L. Stevens  
6311 C. Mora  
6312 F. W. Bingham  
6313 T. E. Blejwas  
6314 J. R. Tillerson  
6315 L. E. Shephard  
6316 R. P. Sandoval  
6317 S. Sinnock  
6332 WMT Library (20)  
6410 N. R. Ortiz  
3141 S. A. Landenberger (5)  
3151 W. I. Klein (3)  
8524 J. A. Wackerly  
3154-1 C. L. Ward (8)  
for DOE/OSTI